Chapter 2
Theory of Quantum-Dot Optical Devices

2.1 Introduction

Modern semiconductor optical devices can consist of a complex arrangement of several different semiconductor crystal layers. By further processing, the semiconductor structure is then shaped into the desired device geometry. Additional steps, such as planarization and contacting, are then required to yield the final usable device. Naturally, a complete microscopic description of the resulting object in all its degrees of freedom is not tractable. Therefore, a restriction to only few degrees of freedom is required, while still maintaining all necessary aspects determining the system behavior.

In the theoretical description of quantum-dot semiconductor optical devices, this means a restriction to the active region, i.e., the parts where the light-matter interaction occurs, and the immediate surrounding matter. Since the optical interactions between the electric field and charge carriers (electrons and holes) are being considered, dynamic equations for these quantities must be derived.

There exist theoretical models for quantum-dot lasers on varying levels of sophistication. Microscopic models that take into account the exact band structure and many-body interactions [1–4] can describe the complex energy structure of quantum dots very realistically, but these approaches are too complicated to be applied in dynamic problems. On the other hand, simple rate-equation models exist [5–7] that can be easily implemented and require little computation power, and often allow for analytical treatment. These models, however, are prone to oversimplification, possibly neglecting important aspects that would lead to different results. In between these two types of approaches there exist multi-rate equation models [8–11], that take into account the delicate energy structure of quantum-dot active media. These models offer a balance between complexity and practicability. In this spirit, we will develop a quantum-dot laser model that takes into account the most important effects needed to realistically describe the laser behavior, while still being simple enough for thorough dynamic studies.

B. Lingnau, *Nonlinear and Nonequilibrium Dynamics of Quantum-Dot Optoelectronic Devices*, Springer Theses, DOI 10.1007/978-3-319-25805-8_2

This chapter presents the derivation of the microscopically based balance equation model that we will use to model the quantum-dot laser and amplifier devices later on in this work. The charge carrier exchange between the quantum-dots and the surrounding material, forming the carrier reservoir, will be described in terms of microscopically based Boltzmann scattering rates, based on carrier-carrier Auger-scattering. The light-matter interaction within the active region will be formulated using a Maxwell–Bloch approach, which we will use to describe the individual contributions of the relevant optical transitions to the optical gain and carrier-induced refractive-index change. Finally, a self-consistent charge-carrier heating model will be presented, in order to dynamically describe the charge-carrier quasi-equilibrium temperature within the quantum-dot device.

2.2 Charge-Carrier Scattering in Quantum-Dot Structures

In electrically operated semiconductor structures, electrons and holes are injected into the medium at the respective contacts. The charge carriers then reach the active region by transport processes due to the applied voltage [12]. In order to reach the energetically lower states, the charge carriers must lose some of their energy. This transfer of energy is realized by means of scattering processes. Here, two different types of charge-carrier scattering can be distinguished: scattering involving only charge carriers and scattering of charge carriers with the environment, most importantly lattice phonons. The scattering mechanisms are illustrated in Fig. 2.1.

Independent of the underlying scattering mechanism, any system will be driven towards an equilibrium state over time. Considering that the fundamental operating principle of lasers—stimulated emission of photons—relies on the inversion of the charge carrier distribution, there always exists a strong nonequilibrium between valence and conduction band electrons. Nevertheless, assuming that the intra-band scattering processes happen on a timescale faster than the inter-band carrier

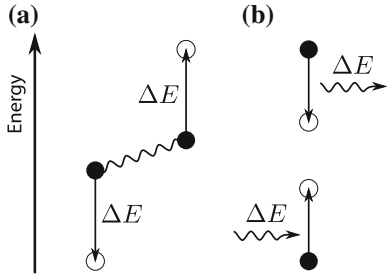

Fig. 2.1 Scattering mechanisms in semiconductor structures. **a** Auger-scattering: an electron scatters into a free energetically lower state under transfer of the energy difference ΔE to another electron. **b** Carrier-phonon scattering: an electron emits a phonon with energy ΔE and scatters into a free state ΔE below its initial state. The reverse process is possible under absorption of a phonon

recombination, it is possible to reach a quasi-equilibrium of the electron distributions in each of the bands. As electrons are fermions, this distribution can then be expressed as a quasi-Fermi distribution:

$$\rho^{\mathrm{eq}}(\varepsilon) = \left[1 + \exp\left(\frac{\varepsilon - E_{\mathrm{F}}^{\mathrm{eq}}}{k_{\mathrm{B}} T^{\mathrm{eq}}}\right)\right]^{-1}, \tag{2.1}$$

with the energy of the corresponding state ε, Boltzmann's constant k_{B}, the quasi-equilibrium temperature T^{eq}, and the quasi-Fermi level $E_{\mathrm{F}}^{\mathrm{eq}}$ relative to the corresponding band edge. As the charge carriers are only in quasi-equilibrium, $E_{\mathrm{F}}^{\mathrm{eq}}$ can differ between conduction and valence band.

The most important scattering mechanism for carrier-carrier scattering is the Coulomb interaction between the charged particles. Since in each scattering event the total energy must be conserved, the scattering of one carrier to a lower state must be accompanied by the scattering of the scattering partner to a higher energy with equal energy difference. This type of process is known as Auger-scattering [12, 13]. Since the total energy of the charge carriers is conserved, Auger-scattering will lead to a change of charge-carrier temperature. A filling of vacant states that lie below the average energy of the electron gas is accompanied by a promotion of other electrons to higher states, such that the total energy is conserved. This effectively broadens the electron distribution, which is equivalent to an increase in temperature and known as Auger-heating [14–19], illustrated in Fig. 2.2.

Apart from the direct interaction between charge carriers, scattering with phonons in the semiconductor lattice is also possible. Here, the charge carriers either absorb or emit energy by interacting with the semiconductor lattice. Contrary to the Auger-scattering mechanism, the scattering with phonons does not conserve the total charge-carrier energy. Thus, a cooling of the charge-carrier distribution towards the lattice temperature is possible.

The theoretical description of the charge-carrier scattering processes can be done on different levels of sophistication. The simplest approach would be a

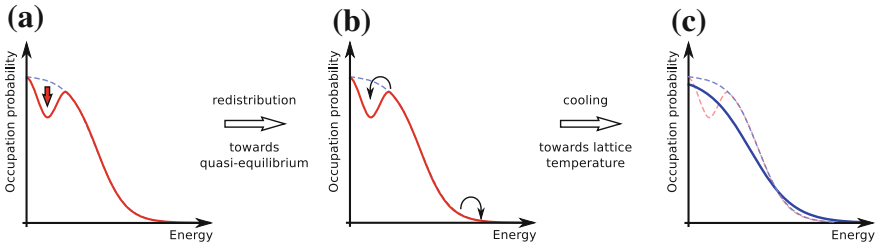

Fig. 2.2 Illustration of carrier heating by Auger-scattering. **a** An initial nonequilibrium electron distribution (*solid line*) is created from quasi-equilibrium (*dashed*). **b** It is then driven towards quasi-equilibrium by Auger-scattering processes. **c** The filling of vacant states at low energy is accompanied by a filling of higher energy states, broadening the resulting quasi-Fermi distribution (*solid line*)

phenomenological description of the scattering by introducing a (constant) scattering time constant at which the charge-carrier population is driven towards a target distribution. On the other end of the spectrum, a microscopic quantum-kinetic description of the many-body system allows a realistic modeling of the scattering dynamics. The drawback of such an approach is of course the enormous computational effort in keeping track of such a high-dimensional system.

Here, an intermediate approach will be pursued, such that the numerical handling of the scattering remains manageable, while the underlying physical processes are still accurately taken into account.

2.2.1 Coulomb-Scattering of Charge Carriers

The starting point for calculating the carrier-carrier scattering is the system Hamiltonian in second quantization [20],

$$H_{\mathrm{sys}} = H_{\mathrm{kin}} + H_{\mathrm{C}} = \sum_{\substack{a \\ s}} \varepsilon_a a^\dagger_{as} a_{as} + \frac{1}{2} \sum_{\substack{abcd \\ ss'}} V_{abcd}\, a^\dagger_{as} a^\dagger_{bs'} a_{cs'} a_{ds}, \tag{2.2}$$

where a_x, $a_x^\dagger$ are the electron annihilation and creation operators in the state x with the energy ε_x, respectively. The Hamiltonian consists of the kinetic contribution H_{kin}, and the Coulomb-interaction Hamiltonian H_{C}. In the sums a, b, c, d denote all possible electron states, with s, s' denoting their spins. The Coulomb interaction matrix element is given by

$$V_{abcd} = \iint \mathrm{d}\boldsymbol{r}\, \mathrm{d}\boldsymbol{r}'\, \phi^*_a(\boldsymbol{r}) \phi^*_b(\boldsymbol{r}') \frac{{e_0}^2}{4\pi\varepsilon_0\varepsilon_{\mathrm{bg}}|\boldsymbol{r} - \boldsymbol{r}'|} \phi_c(\boldsymbol{r}') \phi_d(\boldsymbol{r}), \tag{2.3}$$

with the single-particle wave-functions $\phi_x(\boldsymbol{r})$. The vacuum and background permittivity are given by ε_0 and $\varepsilon_{\mathrm{bg}}$, respectively, and $-e_0$ is the electron charge.

The goal now is to describe the change of the electron probability distribution by Coulomb scattering events. To this end, the change of the occupation probability $\rho_{\nu\sigma} \equiv \langle a^\dagger_{\nu\sigma} a_{\nu\sigma} \rangle$ in a specific state ν with spin σ will be derived. By applying Heisenberg's equation of motion and the commutator relations for fermionic operators, one arrives at:

$$\begin{aligned} \frac{\partial}{\partial t} \rho_{\nu\sigma} = \frac{i}{\hbar} \left\langle \left[H_{\mathrm{sys}}, a^\dagger_{\nu\sigma} a_{\nu\sigma} \right] \right\rangle &= -\frac{i}{\hbar} \sum_{\substack{bcd \\ s'}} \langle V_{\nu bcd} a^\dagger_{\nu\sigma} a^\dagger_{bs'} a_{cs'} a_{d\sigma} \rangle - \mathrm{H.c.} \\ &= \frac{2}{\hbar} \sum_{\substack{bcd \\ s'}} \mathrm{Im} \langle V_{\nu bcd} a^\dagger_{\nu\sigma} a^\dagger_{bs'} a_{cs'} a_{d\sigma} \rangle \,. \end{aligned} \tag{2.4}$$

The expectation value of the two-operator expectation value $\rho_{\nu\sigma}$ now couples to a sum of four-operator expectation values. A factorization of these four-operator

terms into products of two-operator expectation values leads to the Hartree–Fock approximation of the many-body Coulomb interaction. Within this approximation, first-order renormalization effects, including band-gap renormalization and Coulomb enhancement can be described [21, 22]. A description of charge-carrier scattering, however, requires the evaluation of higher-order correlations.

The time derivative of the involved four-operator expectation values is again given by Heisenberg's equation of motion:

$$\begin{aligned}\frac{\partial}{\partial t}\langle a^\dagger_{\nu\sigma}a^\dagger_{bs'}a_{cs'}a_{d\sigma}\rangle &= \frac{i}{\hbar}\left\langle\left[H_{\mathrm{sys}}, a^\dagger_{\nu\sigma}a^\dagger_{bs'}a_{cs'}a_{d\sigma}\right]\right\rangle \\ &= \frac{i}{\hbar}(\varepsilon_\nu+\varepsilon_b-\varepsilon_c-\varepsilon_d)\,\langle a^\dagger_{\nu\sigma}a^\dagger_{bs'}a_{cs'}a_{d\sigma}\rangle \\ &\quad+\frac{i}{\hbar}\left\langle\left[H_{\mathrm{C}}, a^\dagger_{\nu\sigma}a^\dagger_{bs'}a_{cs'}a_{d\sigma}\right]\right\rangle. \end{aligned} \tag{2.5}$$

The evaluation of the commutator in the above equation leads to six-operator expectation values, and their time evolution would couple to eight-operator expectation values and so on. Without further approximations, it is therefore not possible to reach a closed set of equations. Thus, in order to get to a closed form, some approximations must be introduced [20]. First, Eq. (2.5) will be solved adiabatically, by assuming a fast evolution to a steady-state, such that $\frac{\partial}{\partial t}\langle a^\dagger_{\nu\sigma}a^\dagger_{bs'}a_{cs'}a_{d\sigma}\rangle = 0$. This is the Markov approximation, i.e., the explicit time evolution of $\langle a^\dagger_{\nu\sigma}a^\dagger_{bs'}a_{cs'}a_{d\sigma}\rangle$ is suppressed and its value is solely determined by the current system state. Thus

$$\langle a^\dagger_{\nu\sigma}a^\dagger_{bs'}a_{cs'}a_{d\sigma}\rangle = -\frac{\left\langle\left[H_{\mathrm{C}}, a^\dagger_{\nu\sigma}a^\dagger_{bs'}a_{cs'}a_{d\sigma}\right]\right\rangle}{(\varepsilon_\nu+\varepsilon_b-\varepsilon_c-\varepsilon_d)+i\hbar\gamma}, \tag{2.6}$$

where an additional phenomenological decay constant γ has been introduced. Applying the limit $\gamma \to 0$ restores the right hand side of Eq. (2.5). This limit is evaluated by applying the Dirac identity

$$\lim_{\gamma\to 0^+}\frac{1}{x+i\gamma} = \frac{1}{x} - i\pi\delta(x). \tag{2.7}$$

The evaluation of the commutator in Eq. (2.6) contains six-operator expectation values. Instead of deriving equations of motion for these six-operator expressions, they will be factorized into products of two-operator expectation values, neglecting higher order correlations. This means that only terms up to second order in the Coulomb potential will be taken into account. The resulting expectation value can be evaluated to yield

$$\begin{aligned}\left\langle\left[H_{\mathrm{C}}, a^\dagger_{\nu\sigma}a^\dagger_{bs'}a_{cs'}a_{d\sigma}\right]\right\rangle = \left[V^*_{\nu bcd} - V^*_{\nu bdc}\delta_{\sigma,s'}\right]\big[&(1-\rho_{\nu\sigma})(1-\rho_{bs'})\rho_{cs'}\rho_{d\sigma} \\ &- \rho_{\nu\sigma}\rho_{bs'}(1-\rho_{cs'})(1-\rho_{d\sigma})\big].\end{aligned} \tag{2.8}$$

Inserting this relation into Eq. (2.6), applying Eq. (2.7) and inserting the resulting expression into Eq. (2.4) then gives the following equation:

$$\frac{\partial}{\partial t}\rho_{\nu\sigma}\big|_{\mathrm{sc}} = \frac{2\pi}{\hbar}\sum_{\substack{bcd\\ s'}} \mathrm{Re}\left[W_{\nu bcd}\left(W^{*}_{\nu bcd} - W^{*}_{\nu bdc}\right)\right]\delta(\varepsilon_\nu + \varepsilon_b - \varepsilon_c - \varepsilon_d)$$
$$\times\left[(1-\rho_{\nu\sigma})(1-\rho_{bs'})\rho_{cs'}\rho_{d\sigma} - \rho_{\nu\sigma}\rho_{bs'}(1-\rho_{cs'})(1-\rho_{d\sigma})\right], \quad (2.9)$$

which describes the Coulomb scattering in the second-order Born–Markov approximation [23–26]. In the above equation the bare Coulomb potential was replaced with the screened potential W, defined via

$$W(|\boldsymbol{r}-\boldsymbol{r}'|) = V(|\boldsymbol{r}-\boldsymbol{r}'|)e^{-\kappa|\boldsymbol{r}-\boldsymbol{r}'|}. \quad (2.10)$$

Here, κ is the screening wavenumber [20, 27], describing the screening of the Coulomb interaction potential by a surrounding charge-carrier plasma, which can be calculated in a self-consistent way [21, 27]. The screening becomes very important at elevated charge-carrier densities where the unscreened Coulomb potential would greatly overestimate the interaction between the charge carriers.

The summation terms in Eq. (2.9) describe the simultaneous scattering of $d \leftrightarrow \nu$ and $c \leftrightarrow b$. The delta-function ensures energy conservation, such that the total energy of the final states equals that of the initial states. The first term in the second line describes the probability to find particles in the corresponding initial states (c, d) and vacant spaces in the final states (ν, b), and the second term describes the corresponding inverse process, leading to a decrease of ρ_ν.

Equation (2.9) can be written in form of a Boltzmann equation,

$$\frac{\partial}{\partial t}\rho(t)\Big|_{\mathrm{sc}} = S^{\mathrm{in}}[1-\rho(t)] - S^{\mathrm{out}}\rho(t) \quad (2.11)$$

combining the summation terms into an in-scattering rate S^{in} and a corresponding out-scattering rate S^{out} which, however, depend on the charge-carrier occupation of all other states.

Scattering Channels in Coupled Quantum-Dot—Quantum-Well Systems

Equation (2.9) gives the general expression for calculating the Coulomb scattering rates. The sums include all possible states, provided they fulfill the energy conserving δ-function. The given quantum-dot-quantum-well system, however, allows the distinction between qualitatively different scattering processes in order to break up the sums in Eq. (2.9) into different parts which can be handled more easily.

Throughout this work, quantum-dots embedded in a quantum-well (dot-in-a-well, DWELL structure) are considered, with two localized quantum-dot states in both the conduction and valence band. Therefore, two general charge-carrier scattering processes can be distinguished: Capture of a quantum-well electron into a confined quantum-dot state, and intra-dot electron relaxation, with their respective inverse

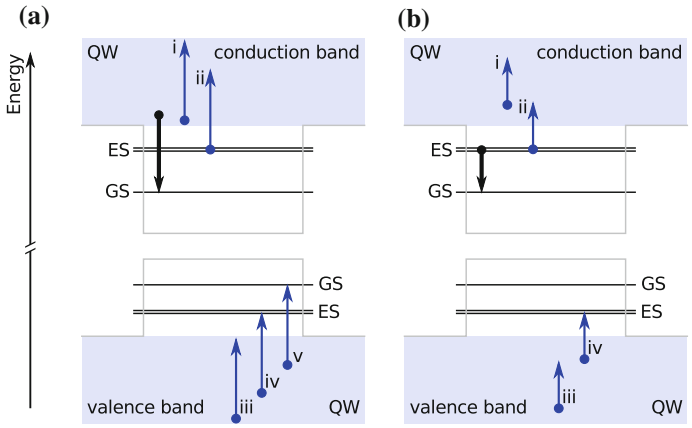

Fig. 2.3 Possible scattering channels in quantum-dot-quantum-well systems. **a** Direct capture into the quantum dot (QD) ground state, **b** Intra-dot relaxation from excited state (ES) to ground-state (GS). The considered electron scattering process is shown by the bold arrow, with the other arrows denoting the possible simultaneous scattering of the Auger-electron to a vacant state: (i) quantum-well (QW) intra-band electron transition, (ii) electron escape from ES to quantum well. The corresponding mixed processes are shown in (iii) and (iv), where the Auger-electron is in the valence band, (v) showing a capture of a valence electron to the GS. For all processes shown, the corresponding reverse scattering is also possible. Not shown is the direct capture into the quantum-dot excited state, analogous to (**a**)

processes. This is illustrated in Fig. 2.3a, b, respectively. The accompanying Auger-process can involve either quantum-well states only, or transitions between quantum-well and other quantum-dot states. Note that depending on the energy difference, not all these scattering channels are possible. For example, in the depicted case of the intra-dot relaxation in Fig. 2.3b, the Auger-transition in the valence band from the quantum well to the ground state is not possible, as it would violate energy conservation. The possible scattering processes contributing to the total scattering rate thus strongly depend on the exact energy scheme of the quantum-dot-quantum-well system. Note that throughout this work impact ionization and Auger-assisted recombination, i.e. the direct scattering between conduction and valence bands, is not considered.

Following the above discussion, the scattering dynamics of the quantum-dot states are rewritten as

$$\begin{aligned}\frac{\partial \rho_{c,\mathrm{GS}}}{\partial t}\Big|_{sc} = {} & S^{\mathrm{cap,in}}_{c,\mathrm{GS}}(\{\rho_{\mathrm{QW}}\})(1-\rho_{c,\mathrm{GS}}) - S^{\mathrm{cap,out}}_{c,\mathrm{GS}}(\{\rho_{\mathrm{QW}}\})\rho_{c,\mathrm{GS}} \\ & + S^{\mathrm{rel,in}}_{c,\mathrm{GS}}(\{\rho_{\mathrm{QW}}\})\rho_{c,\mathrm{ES}}(1-\rho_{c,\mathrm{GS}}) - S^{\mathrm{rel,out}}_{c,\mathrm{GS}}(\{\rho_{\mathrm{QW}}\})(1-\rho_{c,\mathrm{ES}})\rho_{c,\mathrm{GS}},\end{aligned} \tag{2.12a}$$

$$\frac{\partial \rho_{c,\mathrm{ES}}}{\partial t}\Big|_{sc} = S^{\mathrm{cap,in}}_{c,\mathrm{ES}}(\{\rho_{\mathrm{QW}}\})(1-\rho_{c,\mathrm{ES}}) - S^{\mathrm{cap,out}}_{c,\mathrm{ES}}(\{\rho_{\mathrm{QW}}\})\rho_{c,\mathrm{ES}} + S^{\mathrm{rel,in}}_{c,\mathrm{ES}}(\{\rho_{\mathrm{QW}}\})\rho_{c,\mathrm{GS}}(1-\rho_{c,\mathrm{ES}}) - S^{\mathrm{rel,out}}_{c,\mathrm{ES}}(\{\rho_{\mathrm{QW}}\})(1-\rho_{c,\mathrm{GS}})\rho_{c,\mathrm{ES}}. \tag{2.12b}$$

Here, ρ_c denote the electron occupation probabilities of the conduction band states. For valence band states, analogous equations can be written down (subscript v). The scattering rates $S^{\mathrm{cap,in}}$ denote the direct capture of quantum-well electrons into the quantum-dot states, $S^{\mathrm{rel,in}}$ the intra-dot relaxation between the quantum-dot states, with S^{out} being the scattering rate of the respective reverse processes. We can identify the relaxation processes of the excited state with the GS terms,

$$S^{\mathrm{rel,in}}_{c,\mathrm{ES}}(\{\rho_{\mathrm{QW}}\}) = -\frac{1}{2}S^{\mathrm{rel,out}}_{c,\mathrm{GS}}(\{\rho_{\mathrm{QW}}\}), \tag{2.13a}$$

$$S^{\mathrm{rel,out}}_{c,\mathrm{ES}}(\{\rho_{\mathrm{QW}}\}) = -\frac{1}{2}S^{\mathrm{rel,in}}_{c,\mathrm{GS}}(\{\rho_{\mathrm{QW}}\}), \tag{2.13b}$$

with a factor $\frac{1}{2}$ compared to the ground-state contribution, due to its two-fold degeneracy. All scattering rates in above equations depend on the whole quantum-well distribution in both bands, denoted by $\{\rho_{\mathrm{QW}}\}$.

2.2.2 Electron-Hole Picture

It is customary in semiconductor physics to describe the charge carriers in the electron-hole picture, where, starting from a completely filled valence band, an unoccupied state is described as a positively charged hole. The charge-carrier occupations in the conduction and valence bands can then be given in terms of electron and hole populations:

$$\rho_e \equiv \rho_c \tag{2.14a}$$

$$\rho_h \equiv 1-\rho_v. \tag{2.14b}$$

This description leads to a reversed energy axis for holes, leading to a positive effective hole mass. The expressions for the scattering rates is formally identical to the electron picture. The sums in Eq. (2.9), however, now run over both electron and hole states. Using $b \in \{e,h\}$ to distinguish electron and hole states, the scattering dynamics can be written as:

$$\frac{\partial \rho_{b,\mathrm{GS}}}{\partial t}\Big|_{\mathrm{sc}} = S^{\mathrm{cap,in}}_{b,\mathrm{GS}}(\{\rho_{\mathrm{QW}}\})[1-\rho_{b,\mathrm{GS}}] - S^{\mathrm{cap,out}}_{b,\mathrm{GS}}(\{\rho_{\mathrm{QW}}\})\rho_{b,\mathrm{GS}} + S^{\mathrm{rel,in}}_{b}(\{\rho_{\mathrm{QW}}\})\rho_{b,\mathrm{ES}}[1-\rho_{b,\mathrm{GS}}] - S^{\mathrm{rel,out}}_{b}(\{\rho_{\mathrm{QW}}\})[1-\rho_{b,\mathrm{ES}}]\rho_{b,\mathrm{GS}} \tag{2.15a}$$

$$\frac{\partial \rho_{b,\mathrm{ES}}}{\partial t}\Big|_{\mathrm{sc}} = S_{b,\mathrm{ES}}^{\mathrm{cap,in}}(\{\rho_{\mathrm{QW}}\})[1-\rho_{b,\mathrm{ES}}] - S_{b,\mathrm{ES}}^{\mathrm{cap,out}}(\{\rho_{\mathrm{QW}}\})\rho_{b,\mathrm{ES}} - \frac{1}{2}\left[S_{b}^{\mathrm{rel,in}}(\{\rho_{\mathrm{QW}}\})\rho_{b,\mathrm{ES}}[1-\rho_{b,\mathrm{GS}}] - S_{b}^{\mathrm{rel,out}}(\{\rho_{\mathrm{QW}}\})[1-\rho_{b,\mathrm{ES}}]\rho_{b,\mathrm{GS}}\right]. \tag{2.15b}$$

One thing to note is that the capture of valence band electrons into the localized quantum-dot states now corresponds to the escape of holes from the quantum-dots, thus reversing the interpretation of in and out-scattering processes in the valence band. The formal structure of the above equation is nevertheless conserved.

2.2.3 Detailed Balance

The derived scattering expressions so far only describe the dynamics of quantum-dot states and their interaction with the quantum-well charge carriers. The dynamics of quantum-well carriers can in principle be expressed by Eq. (2.9) as well. However, this would require resolving all quantum-well states and tracking their population distribution in time, which greatly increases the dimensionality of the system state. This problem can be resolved by assuming a specific distribution of the carrier population within the quantum-well.

The intra-band scattering between quantum-well states is typically in the order of $\approx$100 fs [28–32]. As long as this scattering is faster than the charge-carrier exchange between the quantum well and quantum-dots, the quantum well can be assumed to be in quasi-equilibrium with good accuracy:

$$\rho_{b,\mathrm{QW}}(\varepsilon_{b,\boldsymbol{k}}^{\mathrm{2D}}) \approx f(\varepsilon_{b,\boldsymbol{k}}^{\mathrm{2D}}, E_{\mathrm{F},b}^{\mathrm{eq}}, T^{\mathrm{eq}}) \equiv \left[1+\exp\left(\frac{\varepsilon_{b,\boldsymbol{k}}^{\mathrm{2D}} - E_{\mathrm{F},b}^{\mathrm{eq}}}{k_{\mathrm{B}}T^{\mathrm{eq}}}\right)\right]^{-1}, \tag{2.16}$$

with the corresponding single-particle energies $\varepsilon_{b,\boldsymbol{k}}^{\mathrm{2D}}$ and the quasi-Fermi level $E_{\mathrm{F},b}^{\mathrm{eq}}$. From this quasi-Fermi distribution the 2D-charge-carrier density w_b in the QWs can be calculated, by taking the density of states in the quantum well as

$$\mathcal{D}_b(E) = D_b\Theta(E - E_{b,0}^{\mathrm{QW}}) = \frac{m_b^*}{\pi\hbar^2}\Theta(E - E_{b,0}^{\mathrm{QW}}), \tag{2.17}$$

under the assumption that the quantum-well sub-band spacing is large enough that only the lowest sub-band needs to be taken into account. The energy $E_{b,0}^{\mathrm{QW}}$ is the corresponding quantum-well band edge and Θ is the Heaviside function. The quantum-well charge-carrier density can then be written as

$$w_b = \frac{2}{A_{\mathrm{act}}}\sum_{\boldsymbol{k}^{\mathrm{2D}}}\left[1+\exp\left(\frac{\varepsilon_{b,\boldsymbol{k}}^{\mathrm{2D}} - E_{\mathrm{F},b}^{\mathrm{eq}}}{k_{\mathrm{B}}T^{\mathrm{eq}}}\right)\right]^{-1}$$

$$= \int_{-\infty}^{\infty} \mathrm{d}\varepsilon_{b,\boldsymbol{k}}^{\mathrm{2D}}\, \mathcal{D}_b(\varepsilon_{b,\boldsymbol{k}}^{\mathrm{2D}}) \left[1 + \exp\left(\frac{\varepsilon_{b,\boldsymbol{k}}^{\mathrm{2D}} - E_{\mathrm{F},b}^{\mathrm{eq}}}{k_{\mathrm{B}} T^{\mathrm{eq}}}\right)\right]^{-1}$$

$$= D_b k_{\mathrm{B}} T^{\mathrm{eq}} \ln\left[1 + \exp\left(\frac{E_{\mathrm{F},b}^{\mathrm{eq}} - E_{b,0}^{\mathrm{QW}}}{k_{\mathrm{B}} T^{\mathrm{eq}}}\right)\right], \tag{2.18}$$

where the sum over all quantum-well $\boldsymbol{k}$-states was expressed as the integral over the charge-carrier energy. A_{act} is the active region in-plane area, with the factor 2 accounting for spin degeneracy. By inverting the above expression, the quasi-Fermi level $E_{\mathrm{F},b}^{\mathrm{eq}}$ can be expressed in terms of the charge-carrier density in the quantum well,

$$E_{\mathrm{F},b}^{\mathrm{eq}} = E_{b,0}^{\mathrm{QW}} + k_{\mathrm{B}} T^{\mathrm{eq}} \ln\left[\exp\left(\frac{w_b}{D_b k_{\mathrm{B}} T^{\mathrm{eq}}}\right) - 1\right]. \tag{2.19}$$

Thus, the quantum-well charge-carrier population can be expressed as a function of the carrier density and the quasi-equilibrium temperature:

$$\rho_{b,\mathrm{QW}}(\varepsilon_{b,\boldsymbol{k}}^{\mathrm{2D}}) \equiv \rho_{b,\mathrm{QW}}(\varepsilon_{b,\boldsymbol{k}}^{\mathrm{2D}}, w_b, T^{\mathrm{eq}}) = \left[1 + \exp\left(\frac{\varepsilon_{b,\boldsymbol{k}}^{\mathrm{2D}} - E_{\mathrm{F},b}^{\mathrm{eq}}(w_b, T^{\mathrm{eq}})}{k_{\mathrm{B}} T^{\mathrm{eq}}}\right)\right]^{-1}. \tag{2.20}$$

By entering this relation into the expressions for the scattering rates Eq. (2.9), also the individual scattering rates can be expressed as functions of only the 2D charge-carrier densities w_b and their quasi-equilibrium temperature T^{eq}, eliminating the need to keep track of the microscopic carrier population distributions.

Furthermore, it is now possible to relate the in and out-scattering rates of a given scattering process to each other [9, 12]. The out-scattering contribution in Eq. (2.9) is equivalent to the in-scattering contribution under the replacement $\rho \to 1 - \rho$, which for the quantum well in quasi-equilibrium can be expressed as

$$1 - \rho_{\mathrm{QW}}(\varepsilon_{b,\boldsymbol{k}}^{\mathrm{2D}}) = \rho_{\mathrm{QW}}(\varepsilon_{b,\boldsymbol{k}}^{\mathrm{2D}}) \exp\left(\frac{\varepsilon_{b,\boldsymbol{k}}^{\mathrm{2D}} - E_{\mathrm{F},b}^{\mathrm{eq}}(w_b, T^{\mathrm{eq}})}{k_{\mathrm{B}} T^{\mathrm{eq}}}\right). \tag{2.21}$$

For the quantum-dot scattering processes the out-scattering rates can thus be written as [33]:

$$S_{b,m}^{\mathrm{cap,out}}(w_e, w_h, T^{\mathrm{eq}}) = S_{b,m}^{\mathrm{cap,in}}(w_e, w_h, T^{\mathrm{eq}}) \exp\left(\frac{\varepsilon_{b,m}^{\mathrm{QD}} - E_{\mathrm{F},b}^{\mathrm{eq}}}{k_{\mathrm{B}} T^{\mathrm{eq}}}\right) \tag{2.22a}$$

$$S_{b}^{\mathrm{rel,out}}(w_e, w_h, T^{\mathrm{eq}}) = S_{b}^{\mathrm{rel,in}}(w_e, w_h, T^{\mathrm{eq}}) \exp\left(\frac{\varepsilon_{b,\mathrm{GS}}^{\mathrm{QD}} - \varepsilon_{b,\mathrm{ES}}^{\mathrm{QD}}}{k_{\mathrm{B}} T^{\mathrm{eq}}}\right), \tag{2.22b}$$

where $\varepsilon_{b,m}^{\mathrm{QD}}$ denotes the energy of the localized quantum-dot state, with $m \in \{\mathrm{GS}, \mathrm{ES}\}$ distinguishing between ground and excited state. The out-scattering of charge-carriers thus becomes more probable at elevated charge-carrier temperatures [34, 35]. Note that in the derivation of above expressions, only a quasi-equilibrium within the quantum well must be assumed without making assumptions about the quantum-dot occupations. Equation (2.22) is therefore valid also in nonequilibrium situations between quantum dot and quantum well.

2.2.4 Carrier-Phonon Scattering

Apart from the direct interaction of the charge carriers moving along the semiconductor lattice, an interaction with the lattice itself is possible. This interaction occurs by the excitation of phonons, the quanta of lattice atom oscillations. In polar semiconductors, such as GaAs, this displacement of the ionic lattice atoms leads to the build-up of a polarization field. Charge carriers can thus couple to phonons in a polar semiconductor via the Coulomb interaction.

Two different important types of phonons must be distinguished: longitudinal optical (LO) phonons and longitudinal acoustic (LA) phonons. The difference between the two varieties lies in their dispersion relation $\omega(\boldsymbol{k})$. LO phonons have a constant energy around the Γ-point (wave vector $\boldsymbol{k} = 0$) and are thus dispersionless (for small $\boldsymbol{k}$), while LA phonons show a nearly linear dispersion relation:

$$\omega_{\mathrm{LO}}(\boldsymbol{k}) \approx \text{const.} \qquad \omega_{\mathrm{LA}}(\boldsymbol{k}) \approx v_s|k|, \tag{2.23}$$

where v_s is the speed of sound. The different dispersion relations critically influence the scattering dynamics of charge carriers with these types of phonons. Since both energy and momentum must be conserved in scattering events, LA phonons only allow for an efficient scattering under the condition that both the energy and momentum difference between the initial and final states of a given scattering event match that of the phonon. This greatly limits the number of possible scattering partners. The scattering with LO phonons, on the other hand, is nearly independent of the momenta of a given initial and final state, as long as their energy difference matches the LO phonon energy $\hbar\omega_{\mathrm{LO}}$. While the scattering to transversal optical (TO) phonons is in principle also possible, the transversal oscillation results in a much smaller total electric field strength and thus to only little interaction with electrons [20].

The quantum-mechanical description of the carrier-phonon interaction is commonly expressed by the Fröhlich electron-phonon coupling Hamiltonian [20]:

$$H_{\mathrm{cp}} = \sum_{\substack{ab\boldsymbol{q} \\ s}} \hbar g_{\boldsymbol{q}}^{ab} a_a^\dagger a_b \left(b_{\boldsymbol{q}} + b_{-\boldsymbol{q}}^\dagger\right). \tag{2.24}$$

This Hamiltonian describes the transition between electronic states $b \rightarrow a$ under either the emission of a LO phonon with wave vector $\boldsymbol{q}$ or the absorption of one with wave vector $-\boldsymbol{q}$. The coupling matrix element for these transitions is given by

$$g_{\boldsymbol{q}}^{ab} = \langle a \mid e^{i\boldsymbol{q}\boldsymbol{r}} \mid b \rangle \, g_{\boldsymbol{q}} \tag{2.25}$$

$$g_{\boldsymbol{q}} = \left[\frac{\omega_{\mathrm{LO}} W_q^{3D}}{2\hbar} \left(\frac{1}{\varepsilon_{\infty}^{\mathrm{bg}}} - \frac{1}{\varepsilon_0^{\mathrm{bg}}} \right) \right]^{\frac{1}{2}}. \tag{2.26}$$

Here, $\varepsilon_0^{\mathrm{bg}}$ and $\varepsilon_{\infty}^{\mathrm{bg}}$ describe the static and high-frequency background permittivity of the medium, respectively. W_q^{3D} is the Fourier-transform of the statically screened three-dimensional Coulomb interaction potential,

$$W_q^{3D} = \frac{{e_0}^2}{V \varepsilon_0 \varepsilon_{\mathrm{bg}} (q^2 + \kappa^2)}, \tag{2.27}$$

with the normalization volume V, and the screening wavenumber κ.

Following a similar approach as for the carrier-carrier scattering, we can derive an expression for the charge-carrier scattering by carrier-phonon scattering [24, 36]:

$$\begin{aligned} \frac{\partial}{\partial t} \rho_{\nu\sigma} \Big|_{cp} = 2\pi \sum_{a\boldsymbol{q}} \left| g_{\boldsymbol{q}}^{a\nu} \right|^2 \Big\{ & \delta_{\nu,a+\mathrm{LO}} \Big[(1 - \rho_{\nu\sigma}) \rho_{a\sigma} n_{\mathrm{ph},\boldsymbol{q}} - \rho_{\nu\sigma} (1 - \rho_{a\sigma}) (n_{\mathrm{ph},\boldsymbol{q}} + 1) \Big] \\ & \delta_{\nu,a-\mathrm{LO}} \Big[(1 - \rho_{\nu\sigma}) \rho_{a\sigma} (n_{\mathrm{ph},\boldsymbol{q}} + 1) - \rho_{\nu\sigma} (1 - \rho_{a\sigma}) n_{\mathrm{ph},\boldsymbol{q}} \Big] \Big\}, \end{aligned} \tag{2.28}$$

where $\delta_{\nu,a\pm\mathrm{LO}} \equiv \delta\big(\varepsilon_\nu - (\varepsilon_a \pm \hbar\omega_{\mathrm{LO}})\big)$ describe the possible situations where the state ν lies $\hbar\omega_{\mathrm{LO}}$ above $(+)$ or below $(-)$ the state a. The terms proportional to the phonon number $n_{\mathrm{ph},\boldsymbol{q}}$ account for the processes where a phonon is absorbed, while those including $(n_{\mathrm{ph},\boldsymbol{q}} + 1)$ account for stimulated and spontaneous emission of a phonon.

Phonon scattering plays an important role for intra-band relaxation processes in bulk and quantum-well structures [37] as well as charge-carrier capture processes into quantum wells from the surrounding bulk semiconductor. The continuous density of states of charge carriers in these systems allow for an efficient scattering with phonons due to many possible transitions matching the LO phonon energy. A cooling of the carrier distribution through emission of phonons is therefore possible and occurs typically on timescales ≈5–10 ps in InGaAs quantum-wells [38, 39].

For scattering processes involving quantum-dot states, on the other hand, the δ-function in Eq. (2.28) greatly limits the scattering efficiency. As the quantum-dot levels are at a discrete distance from the quantum-well band edges, they can couple only to a single charge-carrier energy level within the quantum well by LO phonon scattering. In the case that the quantum-dot localization energy exceeds the LO phonon energy, scattering between the quantum dot and quantum well by

phonons becomes possible only by multi-phonon processes, which have a much lower probability to occur, especially at low temperatures [40, 41]. For intra-dot carrier relaxation processes, effective scattering by LO phonons becomes possible only when the quantum-dot level spacing is an integer multiple of the LO phonon energy, which should apply only for a vanishingly small number of QDs in a given semiconductor structure.

However, it has been shown that the Markov approximation, leading to the emergence of the energy conserving δ-function in the scattering rates, can underestimate its actual value [42–44]. This is due to a broadening of the transition probabilities in energy space by non-Markovian dynamics, which makes scattering possible also for energy differences not matching the LO phonon energy exactly. In [45, 46] it is shown that the interplay between Coulomb and carrier-phonon interaction can lead to an enhancement of scattering rates, with the total rate being higher than the sum of the individual processes. This effect becomes especially prevalent for intra-dot relaxation processes, leading to efficient scattering only weakly dependent on the spacing of quantum-dot energy levels. The charge-carrier capture into QDs, on the other hand, was shown to be well described by carrier-carrier scattering for large enough carrier densities, as they are commonly encountered in quantum-dot electro-optical structures.

In the remainder of this work, we therefore neglect the contribution of the carrier-phonon interaction on the quantum-dot scattering dynamics, in order to maintain computational efficiency. The Coulomb carrier-carrier scattering will be taken into account as the dominant scattering process, which describes the charge-carrier dynamics sufficiently accurately while still allowing for a dynamical analysis of the device behavior.

2.3 Light-Matter Interaction

So far we have derived equations describing the charge-carrier dynamics in the quantum-dot optical structure due to scattering events. In this section, the interaction of the semiconductor medium with light will be derived. The description of light can be done within a semi-classical framework, where the light field itself is described by Maxwell's equations using classical fields. This treatment is often sufficient to describe all important effects governing the behavior of macroscopic semiconductor devices [36, 47].

A fully quantum-mechanical description of the light and its interaction with the semiconductor medium can, however, lead to deviations from the semi-classical treatment under certain conditions. This becomes especially evident in the case when only a few quantum-dots or photons are involved in the lasing process [48, 49]. Then, the non-classical light output from quantum-dots can be used, e.g., for creation of entangled photons [50] or single-photon emission [51, 52]. When discussing optical feedback of few-photon quantum-dot lasers, non-classical effects were also found to arise, characterized by a "bunching" of photons [53, 54], that is unaccounted

for in semi-classical models. In this work, we will limit ourselves to macroscopic scales, and thus classical light states. A semi-classical description of the light-matter interaction is thus sufficient.

2.3.1 Electric Field Dynamics

The starting point for the classical description of the electric field dynamics are Maxwell's equations for the dielectric displacement field $\boldsymbol{D}$, the magnetic field $\boldsymbol{B}$, the electric field $\boldsymbol{\mathcal{E}}$, and the magnetizing field $\boldsymbol{H}$:

$$\nabla \cdot \boldsymbol{D}(\boldsymbol{r}, t) = \rho(\boldsymbol{r}, t) \tag{2.29a}$$

$$\nabla \cdot \boldsymbol{B}(\boldsymbol{r}, t) = 0 \tag{2.29b}$$

$$\nabla \times \boldsymbol{\mathcal{E}}(\boldsymbol{r}, t) = -\frac{\partial}{\partial t}\boldsymbol{B}(\boldsymbol{r}, t) \tag{2.29c}$$

$$\nabla \times \boldsymbol{H}(\boldsymbol{r}, t) = \boldsymbol{j} + \frac{\partial}{\partial t}\boldsymbol{D}(\boldsymbol{r}, t), \tag{2.29d}$$

with the free charge-carrier density ρ, the free current density $\boldsymbol{j}$ and the electric displacement and magnetizing field given by

$$\boldsymbol{D}(\boldsymbol{r}, t) = \varepsilon_0 \boldsymbol{\mathcal{E}}(\boldsymbol{r}, t) + \boldsymbol{\mathcal{P}}(\boldsymbol{r}, t), \tag{2.30}$$

$$\boldsymbol{H}(\boldsymbol{r}, t) = \tfrac{1}{\mu_0}\Big(\boldsymbol{B}(\boldsymbol{r}, t) - \boldsymbol{M}(\boldsymbol{r}, t)\Big), \tag{2.31}$$

respectively. $\boldsymbol{\mathcal{P}}$ and $\boldsymbol{M}$ are the medium polarization and magnetization, respectively. Assuming vanishing free carrier density and current, as well as a non-magnetizable medium, Maxwell's equations can be combined to yield the wave equation for the electric field

$$\varepsilon_0\mu_0 \frac{\partial^2}{\partial t^2}\boldsymbol{\mathcal{E}}(\boldsymbol{r}, t) - \Delta\boldsymbol{\mathcal{E}}(\boldsymbol{r}, t) = -\mu_0 \frac{\partial^2}{\partial t^2}\boldsymbol{\mathcal{P}}(\boldsymbol{r}, t), \tag{2.32}$$

with the Laplace operator Δ. Applying the slowly varying wave approximation, one reaches the time derivation of the slowly varying electric field envelope

$$\frac{\partial}{\partial t}E(\boldsymbol{r}, t) = \frac{i\omega}{2\varepsilon_0\varepsilon_{\mathrm{bg}}}P(\boldsymbol{r}, t). \tag{2.33}$$

where E, P are defined via

$$\boldsymbol{\mathcal{E}}(\boldsymbol{r}, t) = \frac{1}{2}\left(E(\boldsymbol{r}, t)e^{i(\boldsymbol{k}\cdot\boldsymbol{r}-\omega t)} + \text{c.c.}\right)\hat{\boldsymbol{e}} \tag{2.34}$$

$$\boldsymbol{\mathcal{P}}(\boldsymbol{r}, t) = \frac{1}{2}\left(P(\boldsymbol{r}, t)e^{i(\boldsymbol{k}\cdot\boldsymbol{r}-\omega t)} + \text{c.c.}\right)\hat{\boldsymbol{e}} + \varepsilon_0\chi_{\mathrm{bg}}\boldsymbol{\mathcal{E}}(r, t), \tag{2.35}$$

with a carrier frequency ω, and a unit vector $\hat{\boldsymbol{e}}$ giving the electric field polarization. The real background susceptibility χ_{bg} accounts for the linear response of the background medium polarization to the incident electric field and yields the background susceptibility $\varepsilon_{\mathrm{bg}} \equiv (1 + \chi_{\mathrm{bg}})$, leading to the background refractive index $n_{\mathrm{bg}} = \sqrt{\varepsilon_{\mathrm{bg}}}$. The remaining contribution from $P(\boldsymbol{r}, t)$ contains the response of the active medium, which in general cannot be assumed to be linear in $\boldsymbol{\mathcal{E}}$, and can also have an imaginary part, leading to absorption or amplification of the electric field. The fields are expanded in terms of plane waves with the wave vector $\boldsymbol{k}$, where $|\boldsymbol{k}| = \frac{\omega n_{\mathrm{bg}}}{c_0}$. The slowly varying envelope functions E, P are in general complex and thus include both the spatial amplitude as well as the phase profile of the fields.

It is often customary to separate the spatial dependence of the electric field from its time dependence,

$$E(\boldsymbol{r}, t) = E(t) u_E(\boldsymbol{r}), \tag{2.36}$$

thus assuming a time-independent electric field profile in space. In a cavity, $u(\boldsymbol{r})$ describes the main cavity mode profile. Equation (2.36) then corresponds to the single-mode approximation. In general optical cavities allow for a higher number of possible modes, especially in Fabry–Perot type cavities. When a description of multi-mode dynamics is required, Eq. (2.36) can be extended to a linear superposition of the different cavity modes [55]. The assumption of a single mode is nevertheless justified in Fabry–Perot microcavity devices, where the mode spacing between longitudinal modes is very large, as well as in distributed feedback (DFB) devices, where optical modes other than the fundamental cavity mode are suppressed [56–58]. In the remainder of this work we therefore assume a single-mode electric field profile.

The expansion of the electric field in terms of a single mode simplifies the description of the electric field dynamics by eliminating its spatial dependence. The polarization field in the active medium can be expanded in a similar way as Eq. (2.36),

$$P(\boldsymbol{r}, t) = P(t) u_P(\boldsymbol{r}) u_E(\boldsymbol{r}), \tag{2.37}$$

under the assumption that the polarization amplitude is in first order proportional to the electric field amplitude and thus to the electric field mode profile. The spatial polarization profile $u_P(\boldsymbol{r}) \in \mathbb{R}$ is defined by the active medium geometry. In general, the spatial extension of electric and polarization field are different, with the electric field often spanning over a larger volume.

Multiplying Eq. (2.33) with $E^*(z, t)$, adding its complex conjugate and integrating over $\boldsymbol{r}$ yields

$$\begin{aligned} \int \mathrm{d}^3 r E^*(z, t) \frac{\partial}{\partial t} E(z, t) + c.c. &= \frac{\partial}{\partial t} |E(t)|^2 \int \mathrm{d}^3 r \, |u_E(\boldsymbol{r})|^2 \\ &= \frac{\omega}{2\varepsilon_0 \varepsilon_{\mathrm{bg}}} \left[i E^*(t) P(t) + c.c. \right] \int \mathrm{d}^3 r |u_E(\boldsymbol{r})|^2 u_P(\boldsymbol{r}), \end{aligned} \tag{2.38}$$

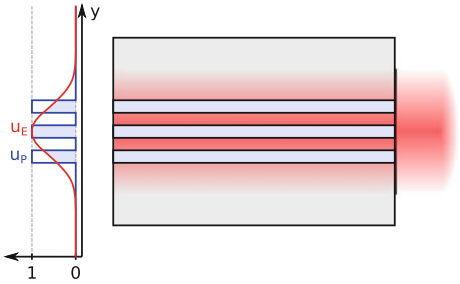

Fig. 2.4 Illustration of the geometric confinement factor. The optical mode profile $u_E(\boldsymbol{r})$ often extends beyond the active medium (*light blue*). The confinement factor describes the overlap of the mode with the active medium distribution $u_P(\boldsymbol{r})$ (color figure online)

which we write as

$$\frac{\partial}{\partial t}|E(t)|^2 = \Gamma \frac{\omega}{2\varepsilon_0 \varepsilon_{\mathrm{bg}}} \left[i E^*(t) P(t) + c.c. \right], \tag{2.39}$$

where we have defined the geometric confinement factor [59]

$$\Gamma = \frac{\int \mathrm{d}^3 r \, |u_E(\boldsymbol{r})|^2 u_P(\boldsymbol{r})}{\int \mathrm{d}^3 r \, |u_E(\boldsymbol{r})|^2}. \tag{2.40}$$

This definition allows one to move the complete spatial dependence of Eq. (2.33) into a single variable Γ. The geometric confinement factor can be understood as the overlap of the active medium with the optical mode, as illustrated in Fig. 2.4. The thus simplified electric field dynamics can be written as

$$\frac{\partial}{\partial t} E(t) = \frac{i\omega\Gamma}{2\varepsilon_0 \varepsilon_{\mathrm{bg}}} P(t). \tag{2.41}$$

Note that Eq. (2.41) does not satisfy Eq. (2.33) at every point in space, but instead only fulfills its space-integrated form. Therefore, only the dynamic evolution of the space-integrated mode amplitude can be described. Changes in the spatial mode profile could in principle occur due to changes of the optical properties of the active medium during operation, e.g., by gain or index guiding effects [60, 61], which could be implemented as a variation of Γ with the operational parameters.

Optical Losses

The electric field inside the optical cavity is subject to losses. Internal optical losses lead to a decay with rate α_{int}, which includes effects such as absorption of photons by free carriers in the surrounding semiconductor material and waveguide losses through the sidewalls. As there exist no perfect mirrors, only a part of the electric field can be reflected back into the cavity, while the rest is transmitted through the cavity mirrors. After each cavity round-trip the electric field is therefore reduced by a factor $r_1 r_2$, with r_1, r_2 denoting the mirror reflectivities at either end of the cavity. Integrating over one cavity round-trip time $\tau_{\mathrm{cav}} = n_{\mathrm{bg}} \ell / c_0$, with the cavity length ℓ,

yields for the polarization-free cavity

$$E(t+\tau_{\mathrm{cav}}) = E(t) r_1 r_2 \exp(-\alpha_{\mathrm{int}}\tau_{\mathrm{cav}}). \tag{2.42}$$

Assuming that τ_{cav} is small compared to all other processes determining the electric field dynamics, the above equation can be transformed to a quasi-continuous change in time:

$$\frac{\partial}{\partial t}E(t)\Big|_{\mathrm{losses}} = -\alpha_{\mathrm{int}}E(t) - \frac{1}{\tau_{\mathrm{cav}}}\ln(r_1 r_2)E(t) \equiv -\kappa E(t), \tag{2.43}$$

where the losses have been combined to a total loss rate κ. Inserting these additional losses into Eq. (2.41), we arrive at the dynamic equation governing the time evolution of the electric field inside the cavity:

$$\frac{\partial}{\partial t}E(t) = \frac{i\omega\Gamma}{2\varepsilon_0\varepsilon_{\mathrm{bg}}}P(t) - \kappa E(t). \tag{2.44}$$

2.3.2 Maxwell–Bloch Equations

So far we have described only the dynamics of the electric field in the cavity, but still missing is the interaction with the active medium. As derived in the previous section, the electric field is driven by the active medium polarization. We will therefore derive expressions for the dynamics of the polarization within the active region in second quantization.

The interaction of the semiconductor matter with the incident light field is described by the dipole interaction Hamiltonian in the electron-hole picture [62], consisting of the kinetic and carrier-field interaction Hamiltonian:

$$\begin{aligned} H &= H_{\mathrm{kin}} + H_{\mathrm{c\text{–}f}} \\ &= \sum_{\substack{c\\s}} \varepsilon_c a^\dagger_{c,s} a_{c,s} + \sum_{\substack{v\\s}} \varepsilon_v d^\dagger_{v,s} d_{v,s} + \sum_{\substack{cv\\s}} \left(\hbar\Omega_{cv} a^\dagger_{c,s} d^\dagger_{v,s} + \mathrm{H.c.}\right), \end{aligned} \tag{2.45}$$

where a, d denote electron and hole annihilator operators, with the summation indices c and v running over all electron and hole states, respectively, with s their spin, and ε_c, ε_v their single-particle energy. The interaction matrix element is defined as

$$\hbar\Omega_{cv} \equiv \langle c \mid -e_0 \boldsymbol{\mathcal{E}}(\boldsymbol{r},t)\cdot\boldsymbol{r} \mid v\rangle = -e_0 \int \mathrm{d}^3 r\, \phi^*_c(\boldsymbol{r})\, \boldsymbol{\mathcal{E}}(\boldsymbol{r},t)\cdot\boldsymbol{r}\, \phi_v(\boldsymbol{r}). \tag{2.46}$$

Assuming that the lateral dimensions of the wave functions of the interacting states are small compared to the electric field wavelength, the electric field can be split off from the matrix element [62], and we can write the carrier-field interaction Hamiltonian

in dipole approximation:

$$H = \sum_{\substack{c \\ s}} \varepsilon_c a^\dagger_{c,s} a_{c,s} + \sum_{\substack{v \\ s}} \varepsilon_v d^\dagger_{v,s} d_{v,s} + \sum_{\substack{cv \\ s}} \left(\mu_{cv} a^\dagger_{c,s} d^\dagger_{v,s} + \text{H.c.}\right) \mathcal{E}(\boldsymbol{r}_{cv}, t), \quad (2.47)$$

with $\boldsymbol{\mathcal{E}} = \mathcal{E}\hat{\boldsymbol{e}}$. The electric field is taken at the coordinate $\boldsymbol{r}_{cv}$, assumed to be the center of mass of the states c, v. The dipole interaction transition moment is defined as

$$\mu_{cv} \equiv \langle c \mid -e_0 \boldsymbol{r} \cdot \hat{\boldsymbol{e}} \mid v \rangle . \quad (2.48)$$

We use Eq. (2.47) to calculate the dynamics of the occupation probabilities $\rho_{e,c,s} \equiv \langle a^\dagger_{c,s} a_{c,s} \rangle$, $\rho_{h,v,s} \equiv \langle d^\dagger_{c,s} d_{c,s} \rangle$, and the inter-band microscopic polarization $\tilde{p}_{cv,s} \equiv \langle d_{h,v,s} a_{e,c,s} \rangle$, by applying Heisenberg's equation of motion. The resulting equations of motion are given by

$$\frac{\partial}{\partial t} \tilde{p}_{cv,s}(t)\Big|_{\text{c–f}} = -i\omega_{cv} \tilde{p}_{cv,s}(t) - i \frac{\mu_{cv} \mathcal{E}(\boldsymbol{r}_{cv}, t)}{\hbar} \left(\rho_{e,c,s}(t) + \rho_{h,v,s}(t) - 1\right), \quad (2.49a)$$

$$\frac{\partial}{\partial t} \rho_{e,c,s}(t)\Big|_{\text{c–f}} = \frac{1}{\hbar} \sum_{v} 2\text{Im}\left(\tilde{p}^*_{cv,s}(t) \mu_{cv} \mathcal{E}(\boldsymbol{r}_{cv}, t)\right), \quad (2.49b)$$

$$\frac{\partial}{\partial t} \rho_{h,v,s}(t)\Big|_{\text{c–f}} = \frac{1}{\hbar} \sum_{c} 2\text{Im}\left(\tilde{p}^*_{cv,s}(t) \mu_{cv} \mathcal{E}(\boldsymbol{r}_{cv}, t)\right), \quad (2.49c)$$

where the inter-band transition frequency is defined by $\omega_{cv} \equiv \frac{1}{\hbar}(\varepsilon_c - \varepsilon_v)$. Inserting the definition of the real electric field $\mathcal{E} = \frac{1}{2}\left(E(\boldsymbol{r}, t) e^{i(\boldsymbol{k}\cdot\boldsymbol{r} - \omega t)} + \text{c.c.}\right)$ into Eq. (2.49), fast oscillating terms $\propto \exp(\pm i\omega t)$ with the carrier frequency ω enter the equations. Let us assume $\omega \approx \omega_{cv}$, i.e., the active medium is excited with light close to the inter-band transition energy. We then move into a co-rotating frame by defining

$$\tilde{p}_{cv,s}(t) \equiv p_{cv,s}(t) e^{i(\boldsymbol{k}\boldsymbol{r}_{cv} - \omega t)} u_E(\boldsymbol{r}_{cv}), \quad (2.50)$$

leading to

$$\frac{\partial}{\partial t} p_{cv,s}(t)\Big|_{\text{c–f}} = -i(\omega_{cv} - \omega) p_{cv,s}(t) - i \frac{\mu_{cv}}{2\hbar} \left(E(t) + E^*(t) e^{-2i(\boldsymbol{k}\boldsymbol{r}_{cv} - \omega t + \phi(\boldsymbol{r}_{cv}))}\right) \times \left(\rho_{e,c,s}(t) + \rho_{h,v,s}(t) - 1\right), \quad (2.51)$$

with $\phi(\boldsymbol{r}) \equiv \arg(u_E(\boldsymbol{r}))$. As ω for infra-red frequencies is in the order of $\approx \text{fs}^{-1}$, which is much faster than the active medium dynamics, the fast oscillating term $\propto E^*(t) e^{2i\omega t}$ can be assumed to average out and is consequently left out. This

approximation is the rotating wave approximation, i.e., $p_{cv,s}$ is assumed to couple only to frequencies close to the inter-band frequency. Furthermore, we assume that only direct inter-band transitions contribute considerably to the light-matter interaction, i.e., any given state c couples only to one specific state v and vice versa. In the quantum-well this corresponds to taking into account only optical transitions without momentum transfer, thus only $p_{\boldsymbol{kk}}$ remain. In the quantum-dots, only transitions p_{GS}, p_{ES} between the electron and hole ground states or excited states, respectively, are kept. The spin index s is from here on suppressed for notational simplicity. Thus, for the slowly varying transition amplitudes p we reach the following coupled equations:

$$\frac{\partial}{\partial t} p_{cv}(t)\Big|_{\text{c–f}} = -i(\omega_{cv} - \omega) p_{cv}(t) - i\frac{\mu_{cv} E(t)}{2\hbar}\left(\rho_{e,c}(t) + \rho_{h,v}(t) - 1\right), \tag{2.52a}$$

$$\frac{\partial}{\partial t} \rho_{e,c}(t)\Big|_{\text{c–f}} = \frac{1}{\hbar}\text{Im}\left(p^*_{cv}(t)\mu_{cv} E(t)|u_E(\boldsymbol{r}_{cv})|^2\right), \tag{2.52b}$$

$$\frac{\partial}{\partial t} \rho_{h,v}(t)\Big|_{\text{c–f}} = \frac{1}{\hbar}\text{Im}\left(p^*_{cv}(t)\mu_{cv} E(t)|u_E(\boldsymbol{r}_{cv})|^2\right). \tag{2.52c}$$

So far, the effects of many-body interactions on the light-matter dynamics has not been taken into account. Similar to the derivations in Sect. 2.2, by including the carrier-carrier and carrier-phonon interaction Hamiltonians for calculating the time-derivatives, these many-body effects can be taken into account. Two types of modifications to the free-carrier results obtained so far can be classified: First-order effects, i.e., terms linear in the interaction matrix elements, lead to changes in the transition energies and the microscopic polarization amplitudes, known as band-gap renormalization and Coulomb enhancement [21, 22, 36, 63, 64]. Second-order effects lead to scattering between charge carriers, as derived earlier for the occupation probabilities. These scattering events not only redistribute charge carriers, but also lead to a decoherence of the involved states and thus to a decay of the microscopic polarization, known as dephasing [65–70]. In the following, these many-body processes are not explicitly taken into account, but instead modeled by a single decay time constant, T_2, characterizing the lifetime of the microscopic polarization. We thus arrive at

$$\begin{aligned}\frac{\partial}{\partial t} p_{cv}(t)\Big|_{\text{c–f}} = &-\left[i(\omega_{cv} - \omega) + \frac{1}{T_2}\right] p_{cv}(t) \\ &- i\frac{\mu_{cv} E(t)}{2\hbar}\left(\rho_{e,c}(t) + \rho_{h,v}(t) - 1\right).\end{aligned} \tag{2.53}$$

Assuming now that the electric field amplitude changes only little over the active region volume, we can set $|u_E(\boldsymbol{r})|$ to be constant. By scaling of $E(t)$ and $p_{cv}(t)$ such that $|u_E(\boldsymbol{r})| = 1$ within the active region, $E(t)$ describes the actual electric

field amplitude in the active region, and the Bloch equations can be simplified to a space-independent form:

$$\left.\frac{\partial}{\partial t} p_{cv}(t)\right|_{\text{c–f}} = -\left[i(\omega_{cv} - \omega) + \frac{1}{T_2}\right] p_{cv}(t) - i\frac{\mu_{cv} E(t)}{2\hbar}\left(\rho_{e,c}(t) + \rho_{h,v}(t) - 1\right), \tag{2.54a}$$

$$\left.\frac{\partial}{\partial t} \rho_{e,c}(t)\right|_{\text{c–f}} = \text{Im}\left(p^*_{cv}(t)\mu_{cv} E(t)\right), \tag{2.54b}$$

$$\left.\frac{\partial}{\partial t} \rho_{h,v}(t)\right|_{\text{c–f}} = \text{Im}\left(p^*_{cv}(t)\mu_{cv} E(t)\right). \tag{2.54c}$$

Defining the macroscopic polarization amplitude as the dipole density,

$$P(t) = \frac{2}{V_{\text{act}}} \sum_{\substack{c \\ s}} \mu^*_{cv} p_{cv}(t), \tag{2.55}$$

where $V_{\text{act}} \equiv \int \text{d}^3 r\, u_P(\boldsymbol{r})$ is the active region volume, we are able to write the electric field dynamics as

$$\frac{\partial}{\partial t} E(t) = \frac{i\omega\Gamma}{2\varepsilon_0 \varepsilon_{\text{bg}}} \frac{2}{V_{\text{act}}} \sum_{\substack{c \\ s}} \mu^*_{cv} p_{cv}(t) - \kappa E(t). \tag{2.56}$$

This equation together with Eq. (2.54) then form the Maxwell–Bloch equations, determining the light-matter interaction in the semiconductor device.

2.4 Quantum-Dot Laser Rate Equations

2.4.1 Maxwell–Bloch Laser Rate Equations

We now apply the previously derived dynamic equations to the considered quantum-dot optoelectronic laser devices. In order to accurately describe its dynamics, the behavior of the optically interacting quantum-dots as well as the charge carriers in the surrounding quantum-well structure must be taken into account. The InAs/InGaAs quantum-dots considered here are supposed to contain two localized electron and hole levels, the energetically lowest one denoted as the ground state, the higher one as excited state. Simpler models treating the quantum-dot confinement potential as a harmonic oscillator potential lead to a two-fold degenerate excited state due to the rotational symmetry with respect to the growth axis [24]. More realistic

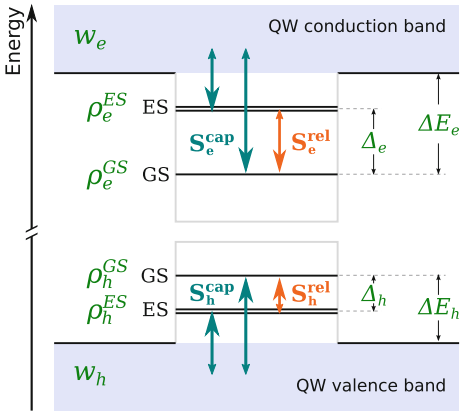

Fig. 2.5 Energy scheme of the considered dot-in-a-well (DWELL) structure. The quantum-dot ground states lie ΔE_b below the quantum-well band edge, with an energy spacing of Δ_b between ground and frist excited state. S_b^{cap} and S_b^{rel} denote direct capture and relaxation scattering processes, respectively

models, however, lift this degeneracy [71]. Nevertheless, the difference in the localization energy between the two first excited states is in the order a few meV, and is thus neglected in the following. Additional to the electronic degeneracy due to the geometric shape of the QDs, all states are assumed to be twofold spin-degenerate. The energy band structure of the considered quantum-dot structure is schematically depicted in Fig. 2.5.

As seen in Sect. 2.2.1, the carrier scattering into the quantum-dot states strongly depends on the occupation of the surrounding carrier reservoir states. Thus, in order to dynamically account for the scattering processes, the charge-carrier dynamics in the reservoir must be taken into account. Following the argumentation of rapid equilibration of the charge carriers within the reservoir states, only the total charge-carrier densities w_e, w_h per unit area in the reservoir must be considered, as the carrier distribution can be calculated from the corresponding quasi-Fermi function.

In the following, let $b \in \{e, h\}$ denote electrons and holes, and $m \in \{\text{GS}, \text{ES}\}$ quantum-dot ground and excited state, respectively, with ν_m their degree of degeneracy, excluding spin. The dynamic equation of the reservoir carrier density can then in general be written as:

$$\frac{\mathrm{d}}{\mathrm{d}t} w_b = \frac{J}{e_0} - r_{\text{loss}}^{w} - \frac{1}{A_{\text{act}}} \sum_{m,i} 2\nu_m \left[S_{b,m,i}^{\text{in,cap}} \rho_{b,m,i} - S_{b,m,i}^{\text{out,cap}} (1 - \rho_{b,m,i}) \right] - \left. \frac{\partial w_b}{\partial t} \right|_{\text{stim}}, \tag{2.57}$$

where J is the electrical pump current density per unit area, e_0 is the electron charge, r_{loss}^{w} is a general loss term, and A_{act} is the area of the active region. The sum runs over all confined quantum-dot states in the mth quantum-dot excited state, denoted

by the index i, with the factor 2 accounting for spin degeneracy. The stimulated recombination contribution is given by

$$\frac{\partial w_b}{\partial t}\Big|_{\text{stim}} = \frac{2}{A_{\text{act}}} \sum_{\boldsymbol{k}^{\text{2D}}} \text{Im}\left(p_{\boldsymbol{k}}^{\text{2D}*}(t) \mu_{\boldsymbol{k}}^{\text{2D}} E(t) \right), \tag{2.58}$$

with the microscopic polarization and dipole moment of the corresponding $\boldsymbol{k}$-state $p_{\boldsymbol{k}}^{\text{2D}}$ and $\mu_{\boldsymbol{k}}^{\text{2D}}$, respectively. Under the assumption that the reservoir charge carriers are in quasi-equilibrium, the dynamic equation for the reservoir polarization can be written as

$$\begin{aligned} \frac{\text{d}}{\text{d}t} p_{\boldsymbol{k}}^{\text{2D}}(t) = &- \left[i(\omega_{\boldsymbol{k}}^{\text{2D}} - \omega) + \frac{1}{T_2} \right] p_{\boldsymbol{k}}^{\text{2D}}(t) \\ &- i \frac{\mu_{\boldsymbol{k}}^{\text{2D}} E(t)}{2\hbar} \left(f(\varepsilon_{e,\boldsymbol{k}}^{\text{2D}}, E_{\text{F},e}^{\text{eq}}, T^{\text{eq}}) + f(\varepsilon_{h,\boldsymbol{k}}^{\text{2D}}, E_{\text{F},h}^{\text{eq}}, T^{\text{eq}}) - 1 \right), \end{aligned} \tag{2.59}$$

with the transition frequency $\omega_{\boldsymbol{k}}^{\text{2D}}$. The losses are modeled as

$$r_{\text{loss}}^{w} = - B^{S} w_e w_h \tag{2.60}$$

with a bimolecular recombination rate B^S [12], accounting for recombination processes of an electron and a hole within the charge-carrier reservoir. The bimolecular recombination of charge carriers in the reservoir is assumed to be the dominant process at the charge-carrier densities encountered in laser devices. In order to model the full carrier-density dependent losses, one would need to take linear losses, e.g., Shockley–Read–Hall recombination via trap states [72], as well as Auger-assisted recombination processes [73] into account.

The sum over all quantum-dot states i in Eq. (2.57) is equivalent to the sum over all quantum-dots within the active region, which would require keeping track of each individual quantum dot as a dynamic variable. As the number of quantum-dots can easily exceed several million within a typical quantum-dot device, Eq. (2.57) must be reformulated.

Individual quantum-dots within the active layer can differ in shape, size, and material composition. The most apparent effect of these inhomogeneities between different quantum-dots is the broadening of the absorption and emission spectra of quantum-dot optical devices. This inhomogeneous broadening is due to the dependence on the transition energy on the aforementioned quantum-dot parameters. While a single quantum dot exhibits sharp transition energies, the quantum-dot ensemble has a continuous spectrum, which can be accurately modeled by a Gaussian distribution function of the quantum-dot energies around a mean value, with a full-width-at-half-maximum (FWHM) of typically some 10 meV [74].

We now characterize each quantum dot by its transition energy, distributing the quantum-dot ensemble into different subgroups, labeled by the index j, with their respective mean transition energy ω_m^j. We introduce the probability mass function

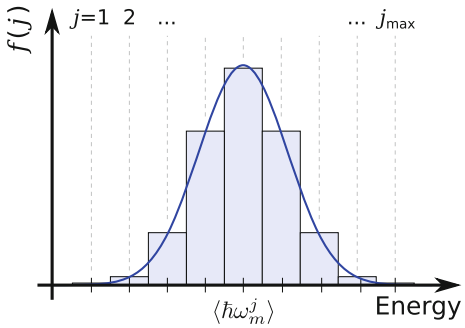

Fig. 2.6 Illustration of the quantum-dot subgroups to model inhomogeneous broadening. The QDs are distributed into $j_{\max}$ subgroups, assumed to follow a Gaussian distribution around the mean transition energy $\langle \hbar\omega_m^j \rangle$. The probability mass function $f(j)$ gives the probability for a quantum dot to be found in the jth subgroup

$f(j)$ denoting the ratio of QDs within the jth subgroup in relation to the total quantum-dot number, as illustrated in Fig. 2.6. Following a Gaussian distribution, $f(j)$ is then given by

$$f(j) = \frac{1}{\mathcal{N}} \exp\left[-4 \ln 2 \left(\frac{\hbar\omega_m^j - \langle \hbar\omega_m^j \rangle}{\Delta E_{\text{inh}}} \right)^2 \right]. \tag{2.61}$$

with the normalization constant $\mathcal{N}$ chosen such that $\sum_j f(j) \overset{!}{=} 1$. For a continuous distribution, one could analytically calculate a closed form for the normalization constant. Due to the discreteness of the subgroups in the simulations, however, $\mathcal{N}$ must be calculated numerically. The inhomogeneous broadening of the optical spectra is given by the sum of the single-particle state broadenings,

$$\Delta E_{\text{inh}} = \Delta\varepsilon_e + \Delta\varepsilon_h, \tag{2.62}$$

where $\Delta\varepsilon_b$ is the corresponding electron and hole state broadening. Only the total broadening ΔE_{inh} is experimentally readily accessible, e.g., by measurements of the quantum-dot luminescence spectra [75]. For the individual state broadening we assume widths proportional to the localization energy of the given state:

$$\Delta\varepsilon_b = \Delta E_{\text{inh}} \frac{\Delta E_b}{\Delta E_e + \Delta E_h}. \tag{2.63}$$

Under the assumption that each quantum dot is fully characterized by its transition energy, i.e., the dynamics of QDs within the same subgroup is identical, the quantum-dot ensemble can be described by a set of dynamic equations for all subgroups. This

assumption is in general only approximately fulfilled, as the energy of the confined quantum-dot states depends on a variety of parameters, such that QDs with equal transition energy do not necessarily have to be identical, and their dynamics could thus differ. By averaging the quantum-dot parameters over the whole ensemble the resulting error should nevertheless be small.

For each quantum-dot subgroup a set of optical Bloch equations can be formulated:

$$\frac{\mathrm{d}}{\mathrm{d}t}p_m^j(t) = -\left[i(\omega_m^j - \omega) + \frac{1}{T_2}\right]p_m^j(t) - i\frac{\mu_m E(t)}{2\hbar}\left(\rho_{e,m}^j(t) + \rho_{h,m}^j(t) - 1\right), \tag{2.64a}$$

$$\frac{\mathrm{d}}{\mathrm{d}t}\rho_{b,m}^j(t) = \frac{1}{\hbar}\mathrm{Im}\left(p_m^{j\,*}(t)\mu_m E(t)\right) - W_m\rho_{e,m}^j(t)\rho_{h,m}^j(t) + \frac{\partial}{\partial t}\rho_{b,m}^j(t)\Big|_{\mathrm{sc}}. \tag{2.64b}$$

The dynamic variables $p_m^j(t)$, $\rho_{m,b}^j(t)$ then describe the inter-band polarization and occupation probabilities of electron and holes in the mth quantum-dot state of the jth subgroup, respectively. In addition to the Bloch equations derived in Eq. (2.54), an additional term accounting for the spontaneous recombination of quantum-dot charge carriers has been introduced, with the recombination rate W_m. The charge-carrier scattering contribution was derived in Eq. (2.15):

$$\frac{\partial}{\partial t}\rho_{b,\mathrm{GS}}^j(t)\Big|_{\mathrm{sc}} = S_{b,\mathrm{GS}}^{j,\mathrm{cap}}(t) + S_b^{j,\mathrm{rel}}(t), \tag{2.65a}$$

$$\frac{\partial}{\partial t}\rho_{b,\mathrm{ES}}^j(t)\Big|_{\mathrm{sc}} = S_{b,\mathrm{ES}}^{j,\mathrm{cap}}(t) - \frac{1}{2}S_b^{j,\mathrm{rel}}(t), \tag{2.65b}$$

with the individual contributions

$$\begin{aligned} S_{b,m}^{j,\mathrm{cap}}(t) &= S_{b,m}^{\mathrm{cap,in}}(w_e, w_h, T^{\mathrm{eq}})[1 - \rho_{b,m}^j(t)] \\ &\quad - S_{b,m}^{\mathrm{cap,out}}(w_e, w_h, T^{\mathrm{eq}})\rho_{b,m}^j(t), \end{aligned} \tag{2.66a}$$

$$\begin{aligned} S_b^{j,\mathrm{rel}}(t) &= S_b^{\mathrm{rel,in}}(w_e, w_h, T^{\mathrm{eq}})[1 - \rho_{b,\mathrm{GS}}^j(t)]\rho_{b,\mathrm{ES}}^j(t) \\ &\quad - S_b^{\mathrm{rel,out}}(w_e, w_h, T^{\mathrm{eq}})\rho_{b,\mathrm{GS}}^j(t)[1 - \rho_{b,\mathrm{ES}}^j(t)]. \end{aligned} \tag{2.66b}$$

Here, $S_{b,m}^{\mathrm{cap,in}}$ and $S_b^{\mathrm{rel,in}}$ describe the quantum-dot in-scattering rates by direct capture from the quantum well and by intra-dot relaxation from the ES to GS, respectively, which depend nonlinearly on the carrier reservoir charge-carrier densities and the quasi-equilibrium carrier temperature. The corresponding out-scattering rates are calculated via detailed balance relations, Eq. (2.22).

We consider only relaxation between quantum-dot states between the ground and excited states of the same quantum-dot subgroup, i.e., we assume a direct mapping of one specific excited state energy to a given ground-state energy. This assumption is strictly valid only if the inhomogeneous broadening of the quantum-dot states is due to the non-uniformity of one specific quantum-dot parameter. As different

quantum-dots might differ, e.g., both in size and shape, it might be possible that any two given quantum-dots share the same ground-state energy but have different excited-state energies, or vice versa. There is an ongoing discussion in the literature whether the assumed one-to-one mapping of ground-state to excited-state energies is valid [76, 77], with experimental results supporting the approximate validity of this assumption. We will therefore only consider the charge-carrier relaxation between equal quantum-dot subgroups.

The dynamic equation for the reservoir charge-carrier densities, Eq. (2.57), can be written as:

$$\frac{\mathrm{d}}{\mathrm{d}t} w_b(t) = \frac{J}{e_0} - r^{w}_{\mathrm{loss}}(t) - 2N^{\mathrm{QD}} \sum_{j,m} \nu_m f(j) S^{j,\mathrm{cap}}_{b,m}(t) - \left.\frac{\partial w_b}{\partial t}\right|_{\mathrm{stim}}, \tag{2.67}$$

where now the sum over all quantum-dot states was replaced by the sum over all quantum-dot subgroups. The sheet density of quantum-dots within the active region per quantum-well layer is given by N^{QD}.

Using Eqs. (2.55) and (2.56), the dynamic equation for the electric field amplitude of the lasing mode can be written as

$$\frac{\partial}{\partial t} E(t) = \frac{i\omega\Gamma}{\varepsilon_0 \varepsilon_{\mathrm{bg}} h^{\mathrm{QW}}} \left[2N^{\mathrm{QD}} \sum_{j,m} \nu_m f(j) \mu^*_m p^j_m + \frac{2}{A_{\mathrm{act}}} \sum_{\boldsymbol{k}^{\mathrm{2D}}} \mu^{\mathrm{2D}*}_k p^{\mathrm{2D}}_k \right] - \kappa E, \tag{2.68}$$

where we used $V_{\mathrm{act}} = a_L A h^{\mathrm{QW}}$, with h^{QW} the height of a single quantum-well layer and a_L the number of quantum-well layers.

2.4.2 Adiabatically Eliminated Polarization

As a further simplification of the previously derived quantum-dot laser model, the dynamics of the microscopic inter-band polarization can be eliminated. The reasoning behind this is the fast dephasing time T_2 of the polarization, which is usually in the order of $\approx$100 fs at room temperature [65, 69, 78]. Considering that the charge-carrier scattering times are commonly in the order of a few ps [24, 26, 45, 79], and the photon lifetime in conventional Fabry–Perot or DFB-type cavities is several ps, this assumption is in many cases justified. All other dynamic variables can then be assumed to be slowly varying, such that the microscopic polarization amplitudes follow a quasi-static relation given by

$$\frac{\mathrm{d}}{\mathrm{d}t} p^j_m(t) = 0. \tag{2.69}$$

Inserting the dynamic equation for the polarization Eq. (2.64a) then yields

$$p_m^j(t) = -iT_2\frac{\mu_m E(t)}{2\hbar}\left(\rho_{e,m}^j(t)+\rho_{h,m}^j(t)-1\right)\left(\frac{1-iT_2(\omega_m^j-\omega)}{1+[T_2(\omega_m^j-\omega)]^2}\right), \quad (2.70)$$

with analogous expressions for the reservoir optical transitions. Inserting this expression in the charge carrier and electric field dynamic equations yields

$$\frac{\partial}{\partial t}\rho_{b,m}^j(t) = -\mathrm{Re}(g_m^j)\left(\rho_{e,m}^j(t)+\rho_{h,m}^j(t)-1\right)|E|^2 - W_m\rho_{e,m}^j(t)\rho_{h,m}^j(t) + \frac{\partial}{\partial t}\rho_{b,m}^j(t)\Big|_{\mathrm{sc}}, \quad (2.71)$$

$$\frac{\partial}{\partial t}E(t) = g(t)E(t) - \kappa E(t), \quad (2.72)$$

with the complex gain coefficient of each subgroup

$$g_m^j = \frac{T_2|\mu_m|^2}{2\hbar^2}\left(\frac{1-iT_2(\omega_m^j-\omega)}{1+[T_2(\omega_m^j-\omega)]^2}\right). \quad (2.73)$$

The gain coefficients $g_{\boldsymbol{k}}^{\mathrm{2D}}$ for the quantum-well inter-band transitions can be written in the same form. Equation (2.73) leads to a Lorentzian-shaped gain spectrum for each individual optical transition, with a FWHM of $2\hbar T_2{}^{-1}$. The corresponding imaginary part of the gain vanishes directly at the transition but becomes large at $\hbar\omega \pm \hbar T_2{}^{-1}$ and then decays slowly towards higher detunings from the carrier frequency ω, as illustrated in Fig. 2.7. This means that for large detuning of the optical field frequency from a given optical transition, the imaginary part of the gain coefficient will predominate. Thus, if we assume the lasing frequency is detuned far enough from the reservoir transitions, we can neglect the real part of the corresponding reservoir gain coefficients. This allows us to neglect the stimulated recombination contribution in the dynamic equation for the reservoir charge-carrier densities:

$$\mathrm{Re}\, g_{\boldsymbol{k}}^{\mathrm{2D}} \approx 0 \quad \Rightarrow \quad \frac{\partial w_b}{\partial t}\Big|_{\mathrm{stim}} \approx 0. \quad (2.74)$$

The resulting complex gain can then be written as

$$g(t) = \frac{\hbar\omega\Gamma}{\varepsilon_0\varepsilon_{\mathrm{bg}}h^{\mathrm{QW}}}\left[2N^{\mathrm{QD}}\sum_{j,m}\nu_m f(j) g_m^j\left(\rho_{e,m}^j(t)+\rho_{h,m}^j(t)-1\right) + \frac{2i}{A_{\mathrm{act}}}\sum_{\boldsymbol{k}^{\mathrm{2D}}}\mathrm{Im}\, g_{\boldsymbol{k}}^{\mathrm{2D}}\left(f(\varepsilon_{e,\boldsymbol{k}}^{\mathrm{2D}}, E_{\mathrm{F},e}^{\mathrm{eq}}, T^{\mathrm{eq}}) + f(\varepsilon_{h,\boldsymbol{k}}^{\mathrm{2D}}, E_{\mathrm{F},h}^{\mathrm{eq}}, T^{\mathrm{eq}}) - 1\right)\right]. \quad (2.75)$$

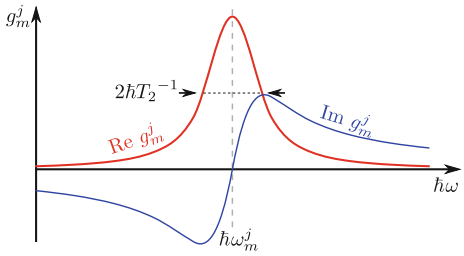

Fig. 2.7 Lorentzian gain profile of a single optical transition. The real part of the quantum-dot gain coefficient g_m^j has a Lorentzian profile around the carrier frequency ω, the imaginary part becomes extremal at $|\omega - \omega_m^j| = {T_2}^{-1}$, while vanishing for resonant transitions $\omega = \omega_m^j$. Note the slower decay of the imaginary part compared to the real part for optical frequencies far from the transition frequency

The downside of using the adiabatically eliminated polarization is the loss of optical frequency dependence. By assuming $\frac{\partial}{\partial t} p_m^j(t) = 0$, the response of the active medium is fixed to a single frequency ω, since p_m^j is the polarization within the rotating frame of the carrier frequency ω. Taking the full polarization dynamics into account, an electric field $E(t) \propto \exp(-i\Delta\omega t)$ would excite optical transitions at any arbitrary frequency $(\omega + \Delta\omega)$. However, the adiabatically eliminated polarization reacts to every electric field as if it was centered at the frequency ω. Thus, when a spectrally broad electric field signal needs to be treated, the full polarization equations must be taken into account. For narrow signals, as, e.g., in single-mode laser devices, the adiabatically eliminated polarization will yield satisfyingly accurate results, with the advantage of lower complexity of the differential equation system.

2.4.3 Modeling of Spontaneous Emission

So far we have only considered the stimulated emission contributing to the electric field in the laser cavity, but have neglected spontaneous emission. In a rigorous derivation, spontaneous emission can only be derived from a fully quantum-mechanical description of the electric field [47, 80], which goes beyond the semi-classical picture used in this work. Instead, we will derive the spontaneous emission terms phenomenologically from energy conservation criteria.

We have written the spontaneous charge-carrier losses in the quantum-dot states as

$$\frac{\partial}{\partial t}\rho_{b,m}^j(t)\Big|_{\mathrm{sp}} = -W_m \rho_{e,m}^j \rho_{h,m}^j. \tag{2.76}$$

The total energy lost by this recombination process can be calculated to

$$2Z^{\mathrm{QD}} \sum_{j,m} \nu_m f(j) W_m \rho_{e,m}^j \rho_{h,m}^j \hbar\omega_m^j, \tag{2.77}$$

with the total quantum-dot number Z^{QD}. We now assume that only a fraction β of the spontaneously recombining charge-carriers emit a photon into the lasing mode. The remaining recombination processes are assumed to either be non-radiative, or emit photons into other modes. The change in the optical energy density $\langle u_{\mathrm{opt}} \rangle$ in the laser mode is thus given by

$$\frac{\partial}{\partial t} \langle u_{\mathrm{opt}} \rangle \Big|_{\mathrm{sp}} = \beta \frac{\Gamma 2 N^{\mathrm{QD}}}{h^{\mathrm{QW}}} \sum_{j,m} \nu_m f(j) W_m \rho^j_{e,m} \rho^j_{h,m} \hbar \omega^j_m. \tag{2.78}$$

From the electric field amplitude, the optical energy density can furthermore be calculated to

$$\langle u_{\mathrm{opt}} \rangle = \frac{\varepsilon_{\mathrm{bg}} \varepsilon_0}{2} |E|^2. \tag{2.79}$$

As the spontaneous emission process can be viewed as a stochastic process with random phase, the contribution to the electric field can be written in terms of a Gaussian white noise process:

$$\frac{\partial}{\partial t} E(t) \Big|_{\mathrm{sp}} = \sqrt{\frac{D_{\mathrm{sp}}}{2}} \xi(t), \tag{2.80}$$

with the complex white noise term $\xi(t) = \xi'(t) + i\xi''(t)$, with $\xi', \xi'' \in \mathbb{R}$, and the spontaneous emission amplitude D_{sp}. The individual terms ξ', ξ'' are assumed to be uncorrelated Gaussian white noise processes. From this the average change in $|E|^2$ can be shown to be [81, 82]:

$$\frac{\partial}{\partial t} \langle |E(t)|^2 \rangle \Big|_{\mathrm{sp}} = D_{\mathrm{sp}}. \tag{2.81}$$

Comparing Eqs. (2.78) and (2.81), the spontaneous emission strength is calculated to

$$D_{\mathrm{sp}} = 2\beta \frac{\Gamma 2 N^{\mathrm{QD}}}{\varepsilon_{\mathrm{bg}} \varepsilon_0 h^{\mathrm{QW}}} \sum_{j,m} \nu_m f(j) W_m \rho^j_{e,m} \rho^j_{h,m} \hbar \omega^j_m. \tag{2.82}$$

Deterministic Approximation

The time-evolution of $|E|^2$ can also be written as

$$\frac{\partial}{\partial t} |E(t)|^2 = 2|E| \frac{\partial}{\partial t} |E|, \tag{2.83}$$

which leads to the deterministic approximation of spontaneous emission:

$$\frac{\partial}{\partial t}E(t)\Big|_{\mathrm{sp}} = \frac{D_{\mathrm{sp}}}{2E^*}. \tag{2.84}$$

While numerically easier to implement than the stochastic approach, this approximation, however, diverges for $E = 0$. A description in the photon picture could circumvent this problem.

2.4.4 Carrier-Induced Gain and Refractive Index Changes

From Eq. (2.72) it becomes clear that the real part of the gain coefficients g_m^j contribute to the amplitude gain or loss of the electric field. The imaginary parts lead to a rotation of $E(t)$ in the complex plane. Since $E(t)$ is the slowly varying amplitude of the electric field in a rotating frame with the carrier frequency ω, the imaginary part of the gain leads to a frequency shift of the electric field towards $\omega - \mathrm{Im}\, g(t)$.

This shift of the electric field frequency induced by interaction with the active medium can be understood as a change in the optical length of the cavity due to a change in refractive index. Writing the total medium susceptibility as

$$\chi(t) = \chi_{\mathrm{bg}} + \delta\chi(t), \tag{2.85}$$

with the charge-carrier-induced susceptibility $\delta\chi$, which is related to the electric field gain via

$$\delta\chi(t) = \frac{2\varepsilon_{\mathrm{bg}}}{i\omega}g(t), \tag{2.86}$$

results in a refractive index

$$\begin{aligned} n(t) &= \sqrt{1+\chi(t)} \\ &= \sqrt{\varepsilon_{\mathrm{bg}} + \frac{2\varepsilon_{\mathrm{bg}}}{i\omega}g(t)} \\ &= n_{\mathrm{bg}}\sqrt{1+\frac{2}{i\omega}g(t)} \\ &\approx n_{\mathrm{bg}}\left(1+\frac{1}{\omega}\mathrm{Im}\, g(t)\right), \end{aligned} \tag{2.87}$$

where in the last line we assumed $|g(t)| \ll \omega$. Considering now a Fabry–Perot cavity of length ℓ, the shifted resonance frequency ω_C of the cavity can be calculated from the resonance condition

$$\begin{aligned}\omega_C(t) &= q\frac{c_0}{2\pi\ell n(t)} \\ &\approx q\frac{c_0}{2\pi\ell n_{\mathrm{bg}}}\left(1-\frac{1}{\omega}\mathrm{Im}\, g(t)\right) \\ &= \omega - \mathrm{Im}\, g(t), \end{aligned} \tag{2.88}$$

with $q \in \mathbb{N}$, and $\omega = qc_0/(2\pi\ell n_{\mathrm{bg}})$. The above shows that the frequency shift of the electric field is due to the shift of the cavity resonance frequency. This argumentation is valid under the assumption of slowly varying $g(t)$ in relation to the cavity round-trip time, i.e., that the build-up of the standing electric field can follow the induced refractive index changes adiabatically.

Equations (2.88) and (2.73) reveal that optical transitions with a higher energy than the considered carrier frequency will lead to a negative non-zero contribution to the imaginary part of the gain. Following Eq. (2.88), these transitions will therefore lead to a blue-shift of the resonance frequency with increasing population by charge carriers. Correspondingly, transitions at lower frequencies than the optical field will lead to a red-shift. By taking into account only the imaginary part of the gain coefficients of the reservoir states in Eq. (2.75), we neglect the optical gain induced by these transitions, but still take into account the induced refractive index changes.

The direct change of the refractive index by charge carriers in the states of the off-resonant transitions is not the only mechanism by which the optical length and thus the resonance frequency of the laser resonator can change. The charge carriers that are lost in non-radiative recombination processes lead to a heating of the semiconductor lattice by emission of phonons in addition to Joule-heating by the applied current. Due to the expansion of the lattice by the increasing temperature the physical length of the resonator increases, leading to a decrease of the resonance frequency and thus a red-shift of the lasing wavelength. This temperature-induced frequency shift is pronounced, e.g., in edge-emitting laser structures, where the active medium runs across the whole length of the laser cavity. The small physical footprint of vertical-cavity surface-emitting lasers (VCSELs) leads to a reduced heat transfer to the surrounding medium or an attached heat sink and subsequently to a pronounced heating of the semiconductor material and a red-shift [83].

Furthermore, not all optical transitions have been accounted for in the present model. In addition to the direct optical transitions already considered, also transitions between confined quantum-dot states and the continuum states of the reservoir involving only conduction band or valence band states are possible. The effect of such transitions on the refractive index can be approximately expressed by a modified Drude formula for the optical susceptibility [84, 85]. In the remainder of this work, we will, however, concentrate on the effects of direct inter-band transitions.

2.5 Quantum-Dot Laser Carrier-Heating Model

Temperature effects in semiconductor optical devices have been previously shown to be important for device design considerations. An increase in lattice and charge-carrier temperature often leads to reduced efficiency and diminished device performance [35, 86]. On the other hand, higher temperatures were shown, e.g., to improve the performance of mode-locked laser devices [87]. Quantum-dot lasers have been theoretically predicted to exhibit lower sensitivity to temperature effects compared to quantum-well devices, due to their confined levels inhibiting thermal escape of optically active carriers to the surrounding reservoir [88]. Experimental findings in some cases confirm an improvement regarding temperature stability, especially in p-doped quantum-dot lasers [89–92], while other results suggest a sensitivity to temperature in quantum-dot lasers that is comparable to quantum-well devices [86, 93]. Taking into account carrier heating and temperature effects can therefore be important for a realistic modeling of quantum-dot optical devices.

In the previous sections, the importance of charge-carrier scattering processes in quantum-dot optical devices has been discussed. The involved Auger processes enter the dynamic equations for the charge-carrier occupations and densities as Boltzmann-like scattering terms. They lead to a redistribution of the charge carriers between the reservoir and quantum-dot states, and, in the process, create so-called hot electrons, which increase the charge carrier distribution temperature. In the following, dynamic equations for the charge-carrier energy and thus the quasi-equilibrium temperature will be derived by formulating energy balance equations for the reservoir charge carriers. These equations can then be used to dynamically include carrier heating in quantum-dot optical devices.

2.5.1 Charge-Carrier Energy and Temperature

As stressed in the previous sections, Auger processes conserve the total charge-carrier energy by redistributing the charge-carrier population. Specifically, when carriers from reservoir states scatter into the lower quantum-dot confined states, energetically higher reservoir states will be occupied by the Auger-electron or hole. A rigorous way to treat this Auger-heating would involve the description of all $\boldsymbol{k}$-states in the reservoir and resolving every possible scattering process in order to determine the dynamic change of each $\boldsymbol{k}$-state. As was detailed previously, such an approach would be numerically very expensive.

Nevertheless, under the assumption of fast quasi-equilibration of the reservoir carrier distributions, an alternative treatment of the Auger-induced carrier distribution changes can be formulated. In quasi-equilibrium, the carrier distribution $\rho_{b,\mathrm{QW}}(\varepsilon^{\mathrm{2D}}_{b,\boldsymbol{k}})$ is given by the quasi-Fermi distribution $f(\varepsilon^{\mathrm{2D}}_{b,\boldsymbol{k}}, E^{\mathrm{eq}}_{\mathrm{F},b}, T^{\mathrm{eq}})$. In order to fully characterize the carrier distribution, only the quasi-Fermi level and quasi-equilibrium temperature must be known. While the quasi-Fermi level can be inferred from the

charge-carrier densities in the carrier reservoir, the quasi-equilibrium temperature in most models is assumed to be constant, and thus Auger heating as well as other heating effects are neglected. Here, an energy balance approach is presented that can be used to dynamically calculate the change of the quasi-equilibrium charge-carrier temperature.

Carrier heating has been previously shown to crucially influence the performance of electro-optic devices. For example in quantum-well lasers carrier heating has been shown to contribute to the nonlinear gain compression, i.e., the reduction of differential gain with increasing optical power [94]. In quantum-well optical amplifiers it was shown that Auger-heating leads to a nonuniform carrier temperature along the device [18]. Carrier heating in quantum-dot lasers has a strong impact on the charge-carrier scattering dynamics due to a change in the detailed balance condition Eq. (2.22) with temperature [95], as well as a quantitative change of the Auger-scattering rates [96].

The total kinetic energy density of the charge carriers in the reservoir states can be written as

$$u = \sum_b \int_{-\infty}^{\infty} \mathrm{d}\varepsilon_{b,\boldsymbol{k}}^{\mathrm{2D}}\, \mathcal{D}_b(\varepsilon_{b,\boldsymbol{k}}^{\mathrm{2D}})\, \varepsilon_{b,\boldsymbol{k}}^{\mathrm{2D}}\, \rho_{b,\mathrm{QW}}(\varepsilon_{b,\boldsymbol{k}}^{\mathrm{2D}}), \tag{2.89}$$

which, under the assumption of a quasi-Fermi distribution in the reservoir states, is related to the quasi-equilibrium charge-carrier temperature T^{eq} via

$$u^{\mathrm{eq}} = \sum_b \int_{-\infty}^{\infty} \mathrm{d}\varepsilon_{b,\boldsymbol{k}}^{\mathrm{2D}}\, \mathcal{D}_b(\varepsilon_{b,\boldsymbol{k}}^{\mathrm{2D}})\, \varepsilon_{b,\boldsymbol{k}}^{\mathrm{2D}} \left[1 + \exp\left(\frac{\varepsilon_{b,\boldsymbol{k}}^{\mathrm{2D}} - E_{\mathrm{F},b}^{\mathrm{eq}}}{k_{\mathrm{B}} T^{\mathrm{eq}}}\right)\right]^{-1}. \tag{2.90}$$

In the case of non-degenerate semiconductors, i.e., for small carrier numbers, the charge carrier distribution in the continuum states approximately follow Boltzmann statistics, and the charge carrier energy density and quasi-equilibrium temperature are simply related via

$$\begin{aligned} u^{\mathrm{eq}}(w_e, w_h, T^{\mathrm{eq}})\big|_{\mathrm{Boltzmann}} &\approx \sum_b \int_0^{\infty} \mathrm{d}\varepsilon_{b,\boldsymbol{k}}^{\mathrm{2D}}\, \mathcal{D}_b(\varepsilon_{b,\boldsymbol{k}}^{\mathrm{2D}})\, \varepsilon_{b,\boldsymbol{k}}^{\mathrm{2D}} \exp\left[\frac{E_{\mathrm{F},b}^{\mathrm{eq}} - \varepsilon_{b,\boldsymbol{k}}^{\mathrm{2D}}}{k_{\mathrm{B}} T^{\mathrm{eq}}}\right] \\ &= k_{\mathrm{B}} T^{\mathrm{eq}}(w_e + w_h) \end{aligned} \tag{2.91}$$

where, for simplicity, the corresponding band edge energies were set to zero.

Generally, however, semiconductor optoelectronic devices can exceed the low-density limit and the above approximation cannot be applied. Instead, the full expression Eq. (2.90) which takes the quasi-Fermi statistics into account must be evaluated.

The quasi-Fermi levels in the reservoir $E_{\mathrm{F},b}^{\mathrm{eq}}$ can be expressed in terms of the charge-carrier densities w_b by using Eq. (2.19). The total charge-carrier energy density then becomes a function of the carrier densities and their quasi-equilibrium

temperature: $u^{\mathrm{eq}} \equiv u^{\mathrm{eq}}(w_e, w_h, T^{\mathrm{eq}})$. For constant w_e and w_h, the quasi-equilibrium energy density increases monotonically with the temperature. As such, it is possible to invert the function $u^{\mathrm{eq}}(w_e, w_h, T^{\mathrm{eq}})$ and instead calculate the quasi-equilibrium carrier temperature from the charge-carrier densities and energy density:

$$T^{\mathrm{eq}} \equiv T^{\mathrm{eq}}(w_e, w_h, u^{\mathrm{eq}}). \tag{2.92}$$

In order to calculate the dynamic changes of the charge carrier temperature during operation of the optoelectronic device, dynamic equations for the charge carrier energy must be formulated.

2.5.2 Carrier Heating by Auger-Scattering Processes

The change of the total kinetic charge carrier energy due to Auger-scattering processes can be determined by calculating the net energy change of the reservoir charge carriers involved in each considered scattering process. This is illustrated in Fig. 2.8. In a charge carrier capture event, a quantum-well charge carrier at energy ε_1 (relative to the quantum-well band edge $E_{b,0}^{\mathrm{QW}}$) fills a vacant quantum-dot state with energy $\varepsilon_{\mathrm{QD}}$, under scattering of a quantum-well carrier from ε_2 to the vacant state ε_3, where energy conservation dictates $\varepsilon_3 = \varepsilon_2 + (\varepsilon_1 - \varepsilon_{\mathrm{QD}})$. The total quantum-well energy change is thus $\Delta U^{\mathrm{QW}} = \varepsilon_3 - \varepsilon_2 - \varepsilon_1 = \varepsilon_{\mathrm{QD}}$, and thus equal to the localization energy of the involved quantum-dot state. Similarly, for intra-dot scattering from the excited to the ground state, a net energy equal to the GS-ES separation Δ_b is added to the total quantum-well charge carrier energy.

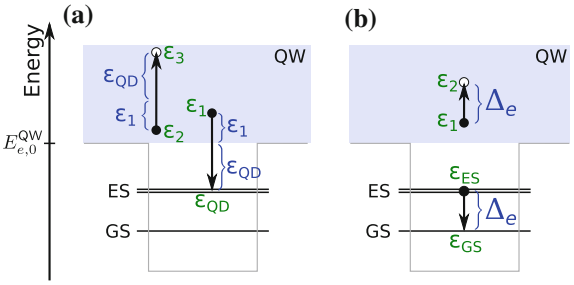

Fig. 2.8 Mechanism of Auger-heating in quantum-dot devices, shown representatively for electrons only. **a** Direct capture processes: a carrier with energy ε_1 relative to the quantum-well (QW) band edge $E_{b,0}^{\mathrm{QW}}$ scatters in to a quantum-dot state $\varepsilon_{\mathrm{QD}}$ below the band edge, while another carrier in the QW gains kinetic energy equal to $\varepsilon_1 + \varepsilon_{\mathrm{QD}}$. The net energy change in the QW is then $\varepsilon_{\mathrm{QD}}$. **b** Relaxation process: a carrier relaxes from the quantum-dot excited state (ES) into the ground state (GS). The Auger electron in the QW adds a net energy of Δ_e to the total QW charge-carrier energy

Considering now all possible Auger-scattering processes in the considered system, the change of the reservoir energy density due to this scattering can be written as:

$$\left.\frac{\partial u}{\partial t}\right|_{\text{Auger}} = \sum_b 2N^{\text{QD}} \sum_{j,m} \nu_m f(j)(E_{b,0}^{\text{QW}} - \varepsilon_{b,m}^{\text{QD},j}) S_{b,m}^{j,\text{cap}} + \sum_j \nu_{\text{GS}} f(j)(\varepsilon_{b,\text{ES}}^{\text{QD},j} - \varepsilon_{b,\text{GS}}^{\text{QD},j}) S_b^{j,\text{rel}}. \tag{2.93}$$

Here, $S_{b,m}^{j,\text{cap}}$ and $S_b^{j,\text{rel}}$ denote the net scattering rates for capture and relaxation processes, respectively, as defined in Eq. (2.66).

2.5.3 Energy Balance Equations

In addition to the above-mentioned contribution of Auger-heating, other mechanisms that influence the charge carrier energy need to be be considered. Not only the scattering of charge carriers with quantum-dot states will change the carrier energy density, but also the scattering of carriers into the reservoir by the pumping process. As the charge carriers can be expected to be thermalized with the lattice when they reach the bulk material surrounding the active medium, the energy gained by the capture of a pump carrier into the reservoir is roughly given by the band-gap energy spacing between the reservoir and bulk materials. We thus assume an average pump energy of $\varepsilon_{\text{pump}}$ per charge carrier. The corresponding contribution to the energy density balance is therefore:

$$\left.\frac{\partial u}{\partial t}\right|_{\text{pump}} = \frac{J}{e_0}\varepsilon_{\text{pump}} \tag{2.94}$$

Furthermore, the spontaneous recombination of charge carriers in the reservoir will effectively remove energy from it. Here, we assume that the recombination is equally probable for all reservoir carriers, i.e., a recombination event will remove twice the average charge carrier energy $\langle u(t)\rangle \equiv u(w_e + w_h)^{-1}$ from the reservoir, as both an electron and a hole are simultaneously annihilated in the process:

$$\left.\frac{\partial u}{\partial t}\right|_{\text{rec}} = \left.\frac{\partial (w_e + w_h)}{\partial t}\right|_{\text{rec}} \langle u(t)\rangle = -\frac{2B^S w_e(t) w_h(t)}{w_e(t) + w_h(t)} u(t) \tag{2.95}$$

Lastly, we have to consider the cooling of the charge carrier gas due to the interaction with lattice phonons. Here, carriers interact with the lattice by emitting a phonon, effectively removing the phonon energy from the total charge carrier energy. This process will cool the carriers towards the lattice temperature T_ℓ. We assume that the

rate of cooling is proportional to the excess energy of the charge carrier gas with respect to the thermal energy it would have at T_ℓ:

$$\frac{\partial u}{\partial t}\Big|_{\text{phon}} = -\gamma_p \left[u(t) - u^{\text{eq}}(w_e, w_h, T_\ell)\right] \tag{2.96}$$

The carrier-phonon interaction rate γ_p is a measure for the timescale on which the carriers are cooled.

Collecting all the above contributions to the energy density balance, we can write the dynamic equation for $u(t)$ as

$$\frac{\mathrm{d}}{\mathrm{d}t}u(t) = \frac{\partial u}{\partial t}\Big|_{\text{pump}} + \frac{\partial u}{\partial t}\Big|_{\text{rec}} + \frac{\partial u}{\partial t}\Big|_{\text{Auger}} + \frac{\partial u}{\partial t}\Big|_{\text{phon}}. \tag{2.97}$$

References

1. W.W. Chow, H.C. Schneider, M.C. Phillips, Theory of quantum-coherence phenomena in semiconductor quantum dots. Phys. Rev. A **68**, 053802 (2003)
2. S. Rodt, A. Schliwa, K. Pötschke, F. Guffarth, D. Bimberg, Correlation of structural and few-particle properties of self-organized InAs/GaAs quantum dots. Phys. Rev. B **71**, 155325 (2005)
3. T. Feldtmann, L. Schneebeli, M. Kira, S.W. Koch, Quantum theory of light emission from a semiconductor quantum dot. Phys. Rev. B **73**, 155319 (2006)
4. C. Gies, J. Wiersig, M. Lorke, F. Jahnke, Semiconductor model for quantum-dot-based microcavity lasers. Phys. Rev. A **75**, 013803 (2007)
5. N.A. Naderi, M. Pochet, F. Grillot, N.B. Terry, V. Kovanis, L.F. Lester, Modeling the injection-locked behavior of a quantum dash semiconductor laser. IEEE J. Sel. Top. Quantum Electron. **15**, 563–571 (2009)
6. L.V. Asryan, R.A. Suris, Upper limit for the modulation bandwidth of a quantum dot laser. Appl. Phys. Lett. **96**, 221112 (2010)
7. T. Erneux, E.A. Viktorov, B. Kelleher, D. Goulding, S.P. Hegarty, G. Huyet, Optically injected quantum-dot lasers. Opt. Lett. **35**, 070937 (2010)
8. C.Z. Tong, S.F. Yoon, C.Y. Ngo, C.Y. Liu, W.K. Loke, Rate equations for 1.3-μm dots-under-a-well and dots-in-a-well self-assembled InAs-GaAs quantum-dot lasers. IEEE J. Quantum Electron. **42**, 1175–1183 (2006)
9. K. Lüdge, E. Schöll, Quantum-dot lasers—desynchronized nonlinear dynamics of electrons and holes. IEEE J. Quantum Electron. **45**, 1396–1403 (2009)
10. M. Gioannini, Ground-state quenching in two-state lasing quantum dot lasers. J. Appl. Phys. **111**, 043108 (2012)
11. C. Wang, B. Lingnau, K. Lüdge, J. Even, F. Grillot, Enhanced dynamic performance of quantum dot semiconductor lasers operating on the excited state. IEEE J. Quantum Electron. **50**, 723–731 (2014)
12. E. Schöll, *Nonequilibrium Phase Transitions in Semiconductors* (Springer, Berlin, 1987)
13. A.V. Uskov, F. Adler, H. Schweizer, M.H. Pilkuhn, Auger carrier relaxation in self-assembled quantum dots by collisions with two-dimensional carriers. J. Appl. Phys. **81**, 7895 (1997)
14. E. Schöll, W. Quade, Effect of impact ionization on hot carrier energy and momentum relaxation in semiconductors. J. Phys. C **20**, L861 (1987)
15. W. Quade, M. Rudan, E. Schöll, Hydrodynamic simulation of impact-ionization effects in p-n junctions. IEEE Trans. CAD **10**, 1287 (1991)

16. W. Quade, E. Schöll, M. Rudan, Impact ionization within the hydrodynamic approach to semiconductor transport. Solid State Electron. **36**, 1493 (1993)
17. P. Borri, S. Ceccherini, M. Gurioli, F. Bogani, Auger heating of carriers in GaAs/AlAs heterostructures. Solid State Commun. **103**, 77–81 (1997)
18. J.N. Fehr, M.A. Dupertuis, T.P. Hessler, L. Kappei, D. Marti, F. Salleras, M.S. Nomura, B. Deveaud, J.-Y. Emery, B. Dagens, Hot phonons and Auger related carrier heating in semiconductor optical amplifiers. IEEE J. Quantum Electron. **38**, 674 (2002)
19. M. Achermann, A.P. Bartko, J.A. Hollingsworth, V.I. Klimov, The effect of auger heating on intraband carrier relaxation in semiconductor quantum rods. Nat. Phys. **2**, 557–561 (2006)
20. G.D. Mahan, *Many-Particle Physics* (Plenum, New York, 1990)
21. H. Haug, S.W. Koch, Semiconductor laser theory with many-body effects. Phys. Rev. A **39**, 1887 (1989)
22. W.W. Chow, S.W. Koch, Theory of semiconductor quantum-dot laser dynamics. IEEE J. Quantum Electron. **41**, 495–505 (2005)
23. H. Haug, A.P. Jauho, *Quantum Kinetics in Transport and Optics of Semiconductors* (Springer, Berlin, 1996)
24. T.R. Nielsen, P. Gartner, F. Jahnke, Many-body theory of carrier capture and relaxation in semiconductor quantum-dot lasers. Phys. Rev. B **69**, 235314 (2004)
25. E. Malić, K.J. Ahn, M.J.P. Bormann, P. Hövel, E. Schöll, A. Knorr, M. Kuntz, D. Bimberg, Theory of relaxation oscillations in semiconductor quantum dot lasers. Appl. Phys. Lett. **89**, 101107 (2006)
26. N. Majer, K. Lüdge, E. Schöll, Cascading enables ultrafast gain recovery dynamics of quantum dot semiconductor optical amplifiers. Phys. Rev. B **82**, 235301 (2010)
27. H. Haug, S. Schmitt-Rink, Electron theory of the optical properties of laser-excited semiconductors. Prog. Quantum Electron. **9**, 3 (1984)
28. R. Binder, D. Scott, A.E. Paul, M. Lindberg, K. Henneberger, S.W. Koch, Carrier-carrier scattering and optical dephasing in highly excited semiconductors. Phys. Rev. B **45**, 1107 (1992)
29. D.B. Tran Thoai, H. Haug, Coulomb quantum kinetics in pulse-excited semiconductors. Z. Phys. B **91**, 199–207 (1992)
30. F.X. Camescasse, A. Alexandrou, D. Hulin, L. Bányai, D.B. Tran Thoai, H. Haug, Ultrafast electron redistribution through Coulomb scattering in undoped GaAs: experiment and theory. Phys. Rev. Lett. **77**, 5429–5432 (1996)
31. M.G. Kane, Nonequilibrium carrier-carrier scattering in two-dimensional carrier systems. Phys. Rev. B **54**, 16345–16348 (1996)
32. L. Bányai, Q.T. Vu, B. Mieck, H. Haug, Ultrafast quantum kinetics of time-dependent RPA-screened Coulomb scattering. Phys. Rev. Lett. **81**, 882–885 (1998)
33. K. Lüdge, Modeling quantum dot based laser devices, in *Nonlinear Laser Dynamics—From Quantum Dots to Cryptography*, ed. by K. Lüdge (WILEY-VCH Weinheim, Weinheim, 2012), chap. 1, pp. 3–34
34. J. Urayama, T.B. Norris, H. Jiang, J. Singh, P. Bhattacharya, Temperature-dependent carrier dynamics in self-assembled InGaAs quantum dots. Appl. Phys. Lett. **80**, 2162–2164 (2002)
35. M. Rossetti, A. Fiore, G. Sek, C. Zinoni, L. Li, Modeling the temperature characteristics of InAs/GaAs quantum dot lasers. J. Appl. Phys. **106**, 023105 (2009)
36. W.W. Chow, S.W. Koch, *Semiconductor-Laser Fundamentals* (Springer, Berlin, 1999)
37. M. Asada, Intraband relaxation time in quantum-well lasers. IEEE J. Quantum Electron. **25**, 2019–2026 (1989)
38. Y.C. Wen, C.Y. Chen, C.H. Shen, S. Gwo, C.K. Sun, Ultrafast carrier thermalization in InN. Appl. Phys. Lett. **89**, 232114 (2006)
39. M. Vallone, Quantum well electron scattering rates through longitudinal optic-phonon dynamical screened interaction: an analytic approach. J. Appl. Phys. **114**, 053704 (2013)
40. T. Inoshita, H. Sakaki, Electron relaxation in a quantum dot: significance of multiphonon processes. Phys. Rev. B **46**, 7260–7263 (1992)
41. J. Feldmann, S.T. Cundiff, M. Arzberger, G. Böhm, G. Abstreiter, Carrier capture into InAs/GaAs quantum dots via multiple optical phonon emission. J. Appl. Phys. **89**, 1180 (2001)

42. J. Seebeck, T.R. Nielsen, P. Gartner, F. Jahnke, Polarons in semiconductor quantum dots and their role in the quantum kinetics of carrier relaxation. Phys. Rev. B **71**, 125327 (2005)
43. J. Seebeck, M. Lorke, P. Gartner, F. Jahnke, Carrier-carrier and carrier-phonon scattering in the low-density and low-temperature regime for resonantly pumped semiconductor quantum dots. Phys. Status Solidi (C) **6**(2), 488–491 (2009)
44. A. Steinhoff, P. Gartner, M. Florian, F. Jahnke, Treatment of carrier scattering in quantum dots beyond the Boltzmann equation. Phys. Rev. B **85**, 205144 (2012)
45. A. Steinhoff, H. Kurtze, P. Gartner, M. Florian, D. Reuter, A.D. Wieck, M. Bayer, F. Jahnke, Combined influence of Coulomb interaction and polarons on the carrier dynamics in InGaAs quantum dots. Phys. Rev. B **88**, 205309 (2013)
46. K. Schuh, P. Gartner, F. Jahnke, Combined influence of carrier-phonon and coulomb scattering on the quantum-dot population dynamics. Phys. Rev. B **87**, 035301 (2013)
47. H. Haken, *Laser Theory* (Springer, Berlin, 1983)
48. S. Ritter, P. Gartner, C. Gies, F. Jahnke, Emission properties and photon statistics of a single quantum dot laser. Opt. Express **18**, 9909 (2010)
49. C. Gies, M. Florian, P. Gartner, F. Jahnke, The single quantum dot-laser: lasing and strong coupling in the high-excitation regime. Opt. Express **19**, 14370 (2011)
50. O. Benson, C. Santori, M. Pelton, Y. Yamamoto, Regulated and entangled photons from a single quantum dot. Phys. Rev. Lett. **84**, 2513–2516 (2000)
51. W. Unrau, D. Quandt, J.H. Schulze, T. Heindel, T.D. Germann, O. Hitzemann, A. Strittmatter, S. Reitzenstein, U.W. Pohl, D. Bimberg, Electrically driven single photon source based on a site-controlled quantum dot with self-aligned current injection. Appl. Phys. Lett. **101**(21), 211119 (2012)
52. G. Callsen, A. Carmele, G. Hönig, C. Kindel, J. Brunnmeier, M. Wagner, E. Stock, J.S. Reparaz, A. Schliwa, S. Reitzenstein, A. Knorr, A. Hoffmann, S. Kako, Y. Arakawa, Steering photon statistics in single quantum dots: from one- to two-photon emission. Phys. Rev. B **87**, 245314 (2013)
53. F. Albert, C. Hopfmann, S. Reitzenstein, C. Schneider, S. Höfling, L. Worschech, M. Kamp, W. Kinzel, A. Forchel, I. Kanter, Observing chaos for quantum-dot microlasers with external feedback. Nat. Commun. **2**, 366 (2011)
54. F. Schulze, B. Lingnau, S.M. Hein, A. Carmele, E. Schöll, K. Lüdge, A. Knorr, Feedback-induced steady-state light bunching above the lasing threshold. Phys. Rev. A **89**, 041801(R) (2014)
55. D. Lenstra, M. Yousefi, Rate-equation model for multi-mode semiconductor lasers with spatial hole burning. Opt. Express **22**, 8143–8149 (2014)
56. H. Kogelnik, C.V. Shank, Coupled-wave theory of distributed feedback lasers. J. Appl. Phys. **43**, 2327–2335 (1972)
57. J. Minch, S.L. Chuang, C.S. Chang, W. Fang, Y.K. Chen, T. Tanbun-Ek, Theory and experiment on the amplified spontaneous emission from distributed-feedback lasers. IEEE J. Quantum Electron. **33**, 815–823 (1997)
58. M. Gioannini, M. Rossetti, Time-domain traveling wave model of quantum dot DFB lasers. IEEE J. Sel. Top. Quantum Electron. **17**, 1318–1326 (2011)
59. Y.Z. Huang, Z. Pan, R.H. Wu, Analysis of the optical confinement factor in semiconductor lasers. J. Appl. Phys. **79**, 3827–3830 (1996)
60. F. Salin, J. Squier, Gain guiding in solid-state lasers. Opt. Lett. **17**, 1352–1354 (1992)
61. N.J. van Druten, S.S.R. Oemrawsingh, Y. Lien, C. Serrat, M.P. van Exter, J.P. Woerdman, Observation of transverse modes in a microchip laser with combined gain and index guiding. J. Opt. Soc. Am. B **18**, 1793–1804 (2001)
62. M.O. Scully, *Quantum Optics* (Cambridge University Press, Cambridge, 1997)
63. H.C. Schneider, W.W. Chow, S.W. Koch, Many-body effects in the gain spectra of highly excited quantum dot lasers. Phys. Rev. B **64**, 115315 (2001)
64. B. Lingnau, K. Lüdge, E. Schöll, W.W. Chow, Many-body and nonequilibrium effects on relaxation oscillations in a quantum-dot microcavity laser. Appl. Phys. Lett. **97**, 111102 (2010)

65. P. Borri, W. Langbein, S. Schneider, U. Woggon, R.L. Sellin, D. Ouyang, D. Bimberg, Ultralong dephasing time in InGaAs quantum dots. Phys. Rev. Lett. **87**, 157401 (2001)
66. H.C. Schneider, W.W. Chow, S.W. Koch, Excitation-induced dephasing in semiconductor quantum dots. Phys. Rev. B **70**, 235308 (2004)
67. H.H. Nilsson, J.Z. Zhang, I. Galbraith, Homogeneous broadening in quantum dots due to Auger scattering with wetting layer carriers. Phys. Rev. B **72**, 205331 (2005)
68. M. Lorke, J. Seebeck, T.R. Nielsen, P. Gartner, F. Jahnke, Excitation dependence of the homogeneous linewidths in quantum dots. Phys. Status Solidi (C) **3**, 2393–2396 (2006)
69. Q.T. Vu, H. Haug, S.W. Koch, Relaxation and dephasing quantum kinetics for a quantum dot in an optically excited quantum well. Phys. Rev. B **73**, 205317 (2006)
70. T. Koprucki, A. Wilms, A. Knorr, U. Bandelow, Modeling of quantum dot lasers with microscopic treatment of Coulomb effects. Opt. Quantum Electron. **42**, 777–783 (2011)
71. A. Schliwa, M. Winkelnkemper, D. Bimberg, Impact of size, shape, and composition on piezoelectric effects and electronic properties of In(Ga)As/GaAs quantum dots. Phys. Rev. B **76**, 205324 (2007)
72. W. Shockley, W.T. Read, Statistics of the recombinations of holes and electrons. Phys. Rev. **87**, 835–842 (1952)
73. A. Beattie, P.T. Landsberg, Auger effect in semiconductors. Proc. R. Soc. A **249**, 16–29 (1959)
74. Y. Nambu, A. Tomita, H. Saito, K. Nishi, Effects of spectral broadening and cross relaxation on the gain saturation characteristics of quantum dot laser amplifiers. Jpn. J. Appl. Phys. **38**, 5087 (1999)
75. W. Lei, M. Offer, A. Lorke, C. Notthoff, C. Meier, O. Wibbelhoff, A.D. Wieck, Probing the band structure of InAs/GaAs quantum dots by capacitance-voltage and photoluminescence spectroscopy. Appl. Phys. Lett. **92**, 193111 (2008)
76. Y. Kaptan, A. Röhm, B. Herzog, B. Lingnau, H. Schmeckebier, D. Arsenijević, V. Mikhelashvili, O. Schops, M. Kolarczik, G. Eisenstein, D. Bimberg, U. Woggon, N. Owschimikow, K. Lüdge, Stability of a quantum dot excited state laser during simultaneous ground state amplification. Appl. Phys. Lett. **105**, 191105-1–191105-4 (2014)
77. Y. Kaptan, H. Schmeckebier, B. Herzog, D. Arsenijević, M. Kolarczik, V. Mikhelashvili, N. Owschimikow, G. Eisenstein, D. Bimberg, U. Woggon, Gain dynamics of quantum dot devices for dual-state operation. Appl. Phys. Lett. **104**, 261108 (2014)
78. P. Borri, W. Langbein, S. Schneider, U. Woggon, R.L. Sellin, D. Ouyang, D. Bimberg, Exciton relaxation and dephasing in quantum-dot amplifiers from room to cryogenic temperature. IEEE J. Sel. Top. Quantum Electron. **8**, 984–991 (2002)
79. A. Wilms, D. Breddermann, P. Mathe, Theory of direct capture from two- and three-dimensional reservoirs to quantum dot states. Phys. Status Solidi (C) **9**, 1278–1280 (2012)
80. R. Loudon, *The Quantum Theory of Light* (Oxford Science Publications, Oxford, 2000)
81. P. Gartner, J. Seebeck, F. Jahnke, Relaxation properties of the quantum kinetics of carrier-LO-phonon interaction in quantum wells and quantum dots. Phys. Rev. B **73**, 115307 (2006)
82. V. Flunkert, E. Schöll, Suppressing noise-induced intensity pulsations in semiconductor lasers by means of time-delayed feedback. Phys. Rev. E **76**, 066202 (2007)
83. Y. Liu, W.-C. Ng, K.D. Choquette, K. Hess, Numerical investigation of self-heating effects of oxide-confined vertical-cavity surface-emitting lasers. IEEE J. Quantum Electron. **41**, 15–25 (2005)
84. A.V. Uskov, E.P. O'Reilly, D. McPeake, D. Bimberg, G. Huyet, N.N. Ledentsov, Carrier-induced refractive index in quantum dot structures due to transitions from discrete quantum dot levels to continuum states. Appl. Phys. Lett. **84**, 272–274 (2004)
85. X. Li, T. Wang, C. Dong, J. Tang, B. Liu, Y. He, Modified Drude model for free-carrier absorption due to bound-to-continuum transition in quantum-dot semiconductor optical amplifier. J. Appl. Phys. **114**, 154506 (2013)
86. D. Klotzkin, P. Bhattacharya, Temperature dependence of dynamic and DC characteristics of quantum-well and quantum-dot lasers: a comparative study. J. Lightwave Technol. **17**, 1634 (1999)

87. M.A. Cataluna, E.A. Viktorov, P. Mandel, W. Sibbett, D.A. Livshits, J. Weimert, A.R. Kovsh, E.U. Rafailov, Temperature dependence of pulse duration in a mode-locked quantum-dot laser. Appl. Phys. Lett. **90**, 101102 (2007)
88. Y. Arakawa, H. Sakaki, Multidimensional quantum well laser and temperature dependence of its threshold current. Appl. Phys. Lett. **40**, 939 (1982)
89. K. Otsubo, N. Hatori, M. Ishida, S. Okumura, T. Akiyama, Y. Nakata, H. Ebe, M. Sugawara, Y. Arakawa, Temperature-insensitive eye-opening under 10-Gb/s modulation of 1.3 μm p-doped quantum-dot lasers without current adjustments. Jpn. J. Appl. Phys. **43**, L1124 (2004)
90. K.T. Tan, C. Marinelli, M.G. Thompson, A. Wonfor, M. Silver, R.L. Sellin, R.V. Penty, I.H. White, M. Kuntz, M. Lämmlin, N.N. Ledentsov, D. Bimberg, A.E. Zhukov, V.M. Ustinov, A.R. Kovsh, High bit rate and elevated temperature data transmission using InGaAs quantum-dot lasers. IEEE Photonics Technol. Lett. **16**, 1415 (2004)
91. S.S. Mikhrin, A.R. Kovsh, I.L. Krestnikov, A.V. Kozhukhov, D.A. Livshits, N.N. Ledentsov, Y.M. Shernyakov, I.I. Novikov, M.V. Maximov, V.M. Ustinov, Z.I. Alferov, High power temperature-insensitive 1.3 μm InAs/InGaAs/GaAs quantum dot lasers. Semicond. Sci. Technol. **20**, 340–342 (2005)
92. M. Sugawara, N. Hatori, M. Ishida, H. Ebe, Y. Arakawa, T. Akiyama, K. Otsubo, T. Yamamoto, Y. Nakata, Recent progress in self-assembled quantum-dot optical devices for optical telecommunication: temperature-insensitive 10 Gbs directly modulated lasers and 40 Gbs signal-regenerative amplifiers. J. Phys. D **38**, 2126–2134 (2005)
93. O.B. Shchekin, G. Park, D.L. Huffaker, D.G. Deppe, Discrete energy level separation and the threshold temperature dependence of quantum dot lasers. Appl. Phys. Lett. **77**(4), 466–468 (2000)
94. J. Wang, H. Schweizer, A quantitative comparison of the classical rate-equation model with the carrier heating model on dynamics of the quantum-well laser: the role of carrier energy relaxation, electron-hole interaction, and Auger effect. IEEE J. Quantum Electron. **33**, 1350–1359 (1997)
95. A.V. Uskov, C. Meuer, H. Schmeckebier, D. Bimberg, Auger capture induced carrier heating in quantum dot lasers and amplifiers. Appl. Phys. Express **4**, 022202 (2011)
96. N. Majer, S. Dommers-Völkel, J. Gomis-Bresco, U. Woggon, K. Lüdge, E. Schöll, Impact of carrier-carrier scattering and carrier heating on pulse train dynamics of quantum dot semiconductor optical amplifiers. Appl. Phys. Lett. **99**, 131102 (2011)

http://www.springer.com/978-3-319-25803-4

Nonlinear and Nonequilibrium Dynamics of
Quantum-Dot Optoelectronic Devices

Lingnau, B.

2015, XIII, 193 p. 88 illus., 25 illus. in color., Hardcover
ISBN: 978-3-319-25803-4